VOLUME 23, 1961/62, No. 3 pp. 69-100 Published 25th January 1962

Philips Technical Review

DEALING WITH TECHNICAL PROBLEMS
RELATING TO THE PRODUCTS, PROCESSES AND INVESTIGATIONS OF
THE PHILIPS INDUSTRIES

NEUTRON DIFFRACTION

by J. A. GOEDKOOP *).

539.125.5:620.179.1

Now that more and more nuclear reactors are being put into operation, neutron diffraction is steadily gaining in importance as a method of analysing crystal structures. One principal reason for this is that neutron diffraction can bring to light certain interesting structural details that are difficult or impossible to determine by X-ray diffraction. Cases in point are the sites of hydrogen atoms and the orientation of magnetic moments.

Since 1952 neutron-diffraction investigations have been carried out with the aid of the nuclear reactor at Kjeller, Norway, as part of the research programme undertaken jointly by the (Norwegian) Institutt for Atomenergi and the (Dutch) Reactor Centrum Nederland. In several cases the structural problems tackled in this programme originated in the Philips Laboratories at Eindhoven, and have been solved with their close cooperation. The present article first describes the technique of neutron diffraction, and goes on to show how this technique has provided important additional data on the structure of three compounds, already investigated by X-ray diffraction at Eindhoven [1]).

Introduction

The structure of a crystalline solid can be investigated with the aid of the diffraction pattern produced when the crystal is irradiated with X-rays. The various methods in use were recently discussed at some length in this journal [1]).

X-radiation is suitable for this purpose because its wavelength is of the same order of magnitude as the interatomic distances in a crystal, that is roughly 1 Å. This being so, a diffraction pattern is produced in which the deflection angles can be measured accurately. This is easily seen from Bragg's equation:

$$2d \sin \Theta = \lambda, \quad \dots\dots \quad (1)$$

where d is the distance between lattice planes, Θ half the angle of deflection and λ the wavelength of the radiation [2]).

Now it is known from wave mechanics that a parallel beam of particles of mass M and velocity v behaves in many respects like a plane wave of wavelength

$$\lambda = h/Mv, \quad \dots\dots \quad (2)$$

where h is Planck's constant. If the mass and velocity of the particles are such that the wavelength is of the order of 1 Å, the phenomena resulting from the passage of these particles through a crystal may be expected to resemble X-ray diffraction phenomena. Shortly after De Broglie put forward equation (2), this was in fact observed from the diffraction of electrons in a crystal. Electron diffraction has since found practical application in the structural analysis of crystals, although it has proved more valuable for investigating the molecular structure of gases. The reason for this is the very high intensity of electron scattering, as a result of which even a small quantity of gas still gives a reasonably measurable diffraction pattern.

---

*) Attached to the Netherlands Reactor Centre at Petten, also Professor Extraordinary of the study of matter with the aid of neutrons at Leyden University.

[1]) P. B. Braun and A. J. van Bommel, X-ray determination of crystal structures, Philips tech. Rev. 22, 126-138, 1960/61 (No. 4).

[2]) The concept "lattice plane" used here differs somewhat from that used in the original formulation of Bragg's law. What was originally the nth-order reflection from a group of lattice planes spaced a distance d' apart, is now a (1st order) reflection from a group of lattice planes whose distance apart is $d = d'/n$. This of course dispenses with the factor n, customarily found in the formulation of Bragg's law.

The development of nuclear reactors has in recent years made another elementary particle available in large quantities for structural analysis, namely the neutron, an uncharged particle having a mass of 1.6×10^{-24} grammes (i.e. roughly the mass of a proton). It is easy to calculate that a wavelength of 1 Å corresponds to neutrons with a velocity of 4 km/sec. It is a fortunate circumstance that a nuclear reactor contains very large amounts of neutrons having velocities near this. These neutrons can be extracted through a channel in the reactor shield.

Since the scattering of neutrons differs in various respects from that of X-radiation, its investigation can serve to supplement structural analysis with X-rays. For this reason neutron diffraction as a method of determining crystal structures has made great progress in recent years. In this article we shall deal first with the experimental and theoretical basis of this method ³). We shall then turn to the three examples described in the above-mentioned article ¹) on X-ray analysis, and show how neutron diffraction has provided additional information in each of these cases.

All experiments were done with the aid of the Kjeller nuclear reactor, Norway, as part of the research programme undertaken jointly by the (Norwegian) Institutt for Atomenergi and the (Dutch) Reactor Centrum Nederland.

The nuclear reactor as a source of neutrons

In a nuclear reactor, neutrons play an essential part as the carriers of the chain reaction ⁴). Upon the splitting of a uranium nucleus that has captured a neutron, other neutrons are liberated, and matters are so arranged in a nuclear reactor that on the average one of these is captured by another uranium nucleus, giving rise to a further fission. The chance of the uranium nuclei capturing a neutron is greater the lower the velocity of the neutron. In most reactors, therefore, the neutrons, which are liberated at very high velocities upon the fission of a nucleus, are decelerated by causing them to collide with the atomic nuclei of a material specially added for that purpose, called the moderator. To slow down the neutrons effectively, these nuclei must be light; moreover they must have no tendency to capture neutrons. Materials meeting these requirements and therefore used in practice as moderators are ordinary water, heavy water (i.e. water containing deuterium instead of hydrogen) and graphite.

As long as the neutrons have a high velocity, they will lose energy upon every collision with an atomic nucleus in the moderator and will thus be slowed down. The nuclei of the moderator, however, are not stationary but are in thermal motion. When the kinetic energy of a neutron has dropped after successive collisions to a value comparable with that of the energy which the moderator atoms possess due to thermal agitation, acceleration as well as deceleration becomes possible. The result is that the neutrons tend to a state of thermal equilibrium with the moderator, and thus move through the latter with the velocities that might be expected for a rarefied gas of atomic weight 1 at the prevailing temperature. Of course, absolute equilibrium is never achieved, since high-energy neutrons are continually added to the system, and moreover low-energy neutrons are absorbed more rapidly than high-energy ones.

The equilibrium distribution of the velocities in such a gas can be derived from the kinetic theory of gases. It is found that, at a temperature of 25 °C, the velocity most frequently occurring is 2200 m/sec, corresponding to a wavelength of 1.8 Å.

Experimental technique of neutron diffraction

The shield around the reactor is fitted with narrow, straight channels, through which neutrons that happen to enter in the right direction can escape freely (*fig. 1*).

In one of the articles referred to above ¹) it is stated that X-ray diffraction patterns are as a rule obtained with *monochromatic* radiation. The neutrons extracted from the reactor, however, have widely differing velocities, corresponding to a wide range of wavelengths. For this reason the first requirement is to select neutrons of the appropriate wavelength from the beam. This is done in a manner familiar in X-ray practice, namely by diffraction: a single crystal (generally a metal crystal) placed in the beam scatters the neutrons in many directions. Each direction corresponds to a different wavelength, determined by the crystal used and its orientation in accordance with Bragg's equation (1). By using such a crystal, a monochromatic beam of the desired wavelength can thus be extracted through an aperture in the shield (fig. 1). This neutron beam, which is of course

---

³) This subject is dealt with at length by G. E. Bacon, Neutron diffraction, Clarendon Press, Oxford 1955; see also C. G. Shull and E. O. Wollan, Applications of neutron diffraction to solid state physics, Part 2, Academic Press, New York 1956; G. R. Ringo, Handbuch der Physik, Part 32, 552, Springer, Berlin 1957.

⁴) See J. J. Went, Philips tech. Rev. **21**, 109, 1959/60.

much weaker than the original one, can then be used in much the same way as a monochromatic beam of X-rays. One can thus, for example, place a single crystal or a powdered specimen in the beam and ascertain the intensity with which the neutrons are scattered in various directions.

Neutrons are not capable of blackening a photographic film. Although there are ways and means of recording a neutron diffraction pattern photographically, in practice neutrons are generally detected by means of a counter tube, a device which is also coming increasingly into use in X-ray diffraction [5]. Since they possess no charge, neutrons cannot cause ionization and thus cannot actuate a counter tube directly. This difficulty is overcome by using a counter tube filled with boron-trifluoride gas. The boron nucleus readily captures neutrons, disintegrating into two charged fragments. The ionizing action of these fragments produces a discharge in the counter tube, so that the number of neutrons entering the tube can be counted.

To determine the intensity distribution in various directions, the neutron counter is mounted on the moving arm of a goniometer, so that it describes an arc around the investigated specimen, on the same principle as in an X-ray diffractometer [6]. Details of the arrangement will be found in fig. 1, which shows the main diffraction set-up at Kjeller [7]. *Fig. 2* shows the equipment in use.

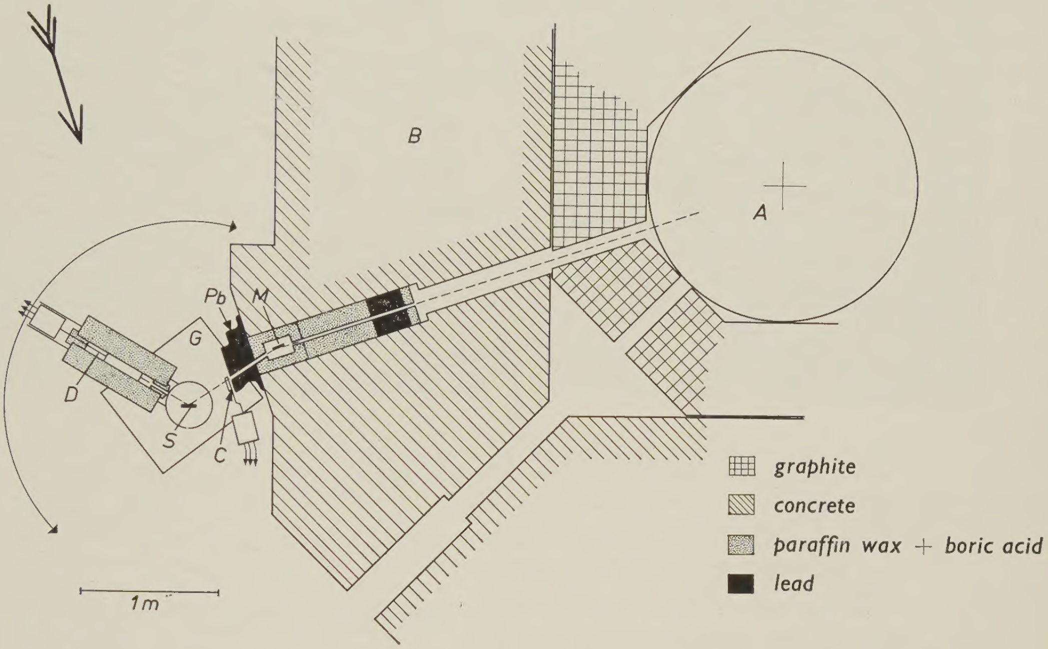

Fig. 1. Diagram of the neutron-diffraction system at Kjeller. The neutrons are extracted from the reactor *A* through a channel in the reactor shield *B*; they encounter in their path a large single crystal of lead *M*, which — still within the shield — scatters them in a number of directions. Neutrons travelling in one specific direction pass through an aperture in the lead shield *Pb*: the whole system thus works as a monochromator. In the arrangement at Kjeller the crystal is so situated that only those neutrons that are reflected by the (111) planes of the crystal pass through the aperture, resulting in a monochromatic beam of wavelength 1.03 Å. The sample *S* to be analysed (single crystal or powder) is mounted on the shaft of a goniometer *G*, around which the BF_3-filled neutron counter *D* can be rotated. The counter is surrounded by a thick shield to protect it from stray neutrons in the reactor building. The apparatus works automatically in steps: when the counter is stationary the number of scattered neutrons is counted during a period in which a specific number of neutrons (e.g. 100 000) are recorded in a small monitor counter *C*, which intercepts part of the monochromatic beam. At the end of this period the number counted is printed on a paper strip and the counter arm is swung through an angle of 0.2°, the slide carrying the sample being shifted through an angle of 0.1°. A new counting period then starts. — Fig. 2 shows a photograph of this set-up taken in the direction of the arrow shown here top left.

---

[5] See W. Parrish, X-ray intensity measurements with counter tubes, Philips tech. Rev. **17**, 206-221, 1955/56.

[6] See W. Parrish, E. A. Hamacher and K. Lowitzsch, Philips tech. Rev. **16**, 123, 1954/55.

[7] For further particulars see J. A. Goedkoop, Ned. T. Natuurk. **23**, 140, 1957.

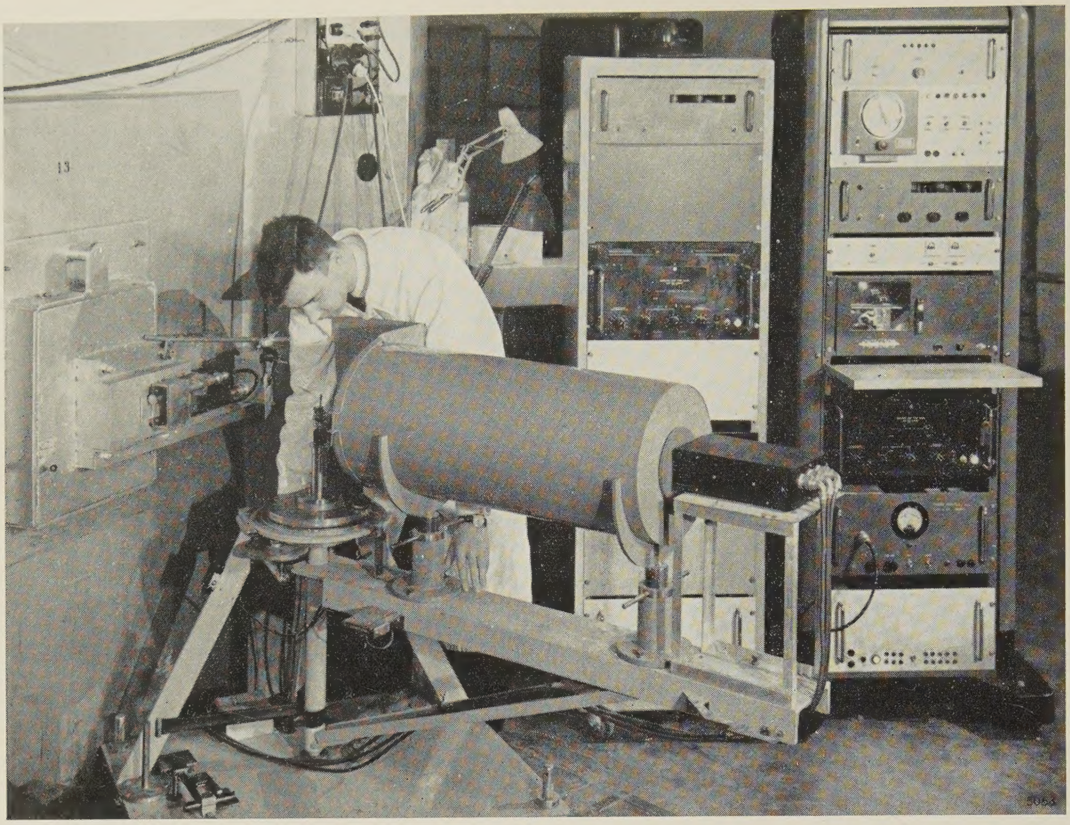

Fig. 2. View of the neutron-diffraction equipment at Kjeller. The direction of observation is indicated by the arrow in fig. 1. The neutron aperture, covered by a plate, is situated in the middle of the lead block at the left-hand side of the picture. The monitor counter can be seen to the right of this aperture. The sample is visible in front of the experimentor's sleeve. The large cylinder is the shield around the neutron counter, which is mounted on a goniometer arm that turns around the same axis as the sample. On the extreme right of the arm can be seen the pre-amplifier for the neutron counter. Under the sample holder can be seen some of the gear wheels of the driving mechanism. The control and recording system is accommodated in two racks in the background. The results are printed on a paper strip in the middle of the right-hand rack. (From: Atoomenergie en haar toepassingen **2**, 82, 1960.)

Neutron scattering by the atomic nucleus

Electromagnetic radiation is scattered by charged particles with an amplitude inversely proportional to the mass of the particle. For this reason X-ray scattering only provides information on the distribution of the *electrons* in a crystal: the atomic nuclei are too heavy to make any perceptible contribution.

In the case of neutron scattering it is the *nuclei* that cause the scatter, whilst the interaction between neutron and electron is very slight (with one important exception, to which we shall return presently).

The neutron, as will be known, is a normal constituent of all atomic nuclei, apart from ^{1}H. The forces acting between a neutron and an atomic nucleus in a collision are of the same nature as those that hold the neutrons and protons together inside the nucleus. A characteristic of these forces is their short range, roughly 10^{-12} cm, which is of the same order of magnitude as the diameter of the atomic nucleus. Since the wavelength at which we are working is about 10^{-8} cm, we can regard the atomic nucleus as a point scatterer, which means that the scattering is isotropic. The scattering action of a given atomic nucleus can thus be described by a single quantity, called the *scattering length* and denoted by the letter *b*.

In order to explain the significance of b, we shall consider a parallel beam of neutrons, containing n neutrons per cm^3, all having the velocity v cm/sec. The neutron flux is then nv, in other words nv neutrons pass per second through unit area perpendicular to the beam.

In terms of wave mechanics the beam is represented by a plane wave of amplitude $\sqrt{n}$ (the square of the absolute value of the wave function must everywhere be equal to the local density). A single atomic nucleus placed in the beam, being a point scatterer, will be the centre of a spherically scattered wave whose amplitude is proportional to $\sqrt{n}$ and inversely proportional to the distance r from the centre of the nucleus. The amplitude may therefore be represented by $(b/r)\sqrt{n}$. We have thus defined the quantity b, which evidently has the dimension of a length.

We may now introduce in this connection another useful concept. It follows from the above that the density of the scattered neutrons at a distance r is equal to $(b/r)^2n$. Supposing the scattering nucleus to be surrounded by a sphere of radius r, the number of scattered neutrons passing through this sphere per second will be

$$4\pi r^2 \times v \times (b/r)^2 n = 4\pi b^2 nv \,. \quad . \quad . \quad . \quad . \quad . \qquad (3)$$

Of the nv neutrons striking an area of 1 cm² the nucleus will thus, as it were, scatter those that are incident on a part $\sigma = 4\pi b^2$ of that area, and the others not at all. The quantity σ is therefore called the *effective scattering cross-section*, and is generally of the same order as the cross-section of the atomic nucleus.

Table I gives the scattering lengths [8]) for the elements with which we shall be concerned in the examples presented in this article. It would be beyond our present scope to deal with the physical factors governing the scattering length. In any case, a quantitative treatment of these factors is not as a rule possible, and in most cases the scattering lengths are determined empirically. We will not discuss this either, and shall thus simply consider the scattering lengths as given quantities in what follows.

Table I. Scattering lengths of some atoms for neutrons and for X-radiation.

Element	Atomic number Z	Neutron scattering length *) b in 10^{-12} cm	X-ray scattering length c in 10^{-12} cm	
			for $\sin\Theta/\lambda = 0$	for $\sin\Theta/\lambda = 0.5\times10^{8}$ cm^{-1}
Hydrogen	1	H: − 0.38 D: 0.65	0.28	0.02
Oxygen	6	0.58	2.25	0.62
Aluminium	13	0.35	3.65	1.55
Manganese	25	−0.37	7.0	3.1
Iron	26	0.96	7.3	3.3
Zinc	30	0.59	8.5	3.9
Barium	56	0.53	15.8	8.3
Thorium	90	1.01	25.2	14.4

*) Hydrogen excepted, these are the scattering lengths for the natural isotopic mixture.

The tabulated values call for some comments, of importance to our subsequent considerations.

a) The various isotopes of an element have different scattering lengths, a fact which is clearly demonstrated by the striking difference between H and D. An average value is taken for the other elements, applicable to the natural isotopic ratio.

b) In two cases, H and Mn, (and in the case of some other elements not mentioned here) the scattering length is negative. The significance of this may be understood when it is realized that the scattered neutron wave can have different phases in relation to the incident wave. In practice, two principal cases arise. At the scattering nucleus, the scattered wave is either in phase with the incident wave or in anti-phase with it. These two cases may be indicated by giving b a positive or negative sign: the phase difference is nearly always 180°, which we indicate by a plus sign; a phase difference of 0° thus corresponds to b negative.

c) Although the scattering lengths in Table I show a definite tendency to increase with increasing Z (as can be seen more clearly from a table for all elements), this increase is not particularly pronounced compared with the very marked irregularities (compare, for example, the neighbours Mn and Fe).

Comparison with X-ray scattering

We have noted that X-rays are scattered by the electrons in a crystal. Consequently, the X-ray-scattering action of an atom increases more or less linearly as the number of electrons increases, that is to say with increasing atomic number Z in the periodic system. If we consider a compound containing e.g. thorium ($Z = 90$) and hydrogen ($Z = 1$), it is evident that the scattering due to the hydrogen will be entirely insignificant compared with that due to the thorium. It will therefore be difficult, if not impossible, to determine by means of X-ray diffraction exactly where the hydrogen is located.

A glance at Table I shows that neutron diffraction gives much more chance of determining the position of the hydrogen nuclei.

It may also happen that a crystal contains two elements that are close together in the periodic system. In that case the electron density will not change appreciably if the two atoms exchange sites, so that it is difficult to distinguish one atom from the other on the basis of the X-ray diffraction pattern. Here, too, neutron diffraction makes more reliable determination possible. A clear case in point is that of Fe and Mn, already mentioned in passing; another example discussed below also demonstrates a third very important difference between X-ray and neutron diffraction, which is that the latter is able to provide information about the magnetic structure of crystals.

Before going into this interesting aspect and discussing examples, we shall pursue for a moment the comparison of neutron and X-ray scattering. Electrons are point scatterers for X-radiation, but the observed X-ray diffraction pattern is necessarily an average over a time in which the electrons have undergone many revolutions. For that reason the picture we get of the electrons is a "smeared" continuous distribution of electrons in space. Something similar, though to a much lesser extent, applies to the nuclei as scatterers of neutrons. As a first approximation the nuclei are located at fixed sites in the crystal; the scattering of neutrons is thus everywhere zero except at the sites of the nuclei (integrating the neutron scattering over the cross-sectional area of the nuclei, we obtain a value proportional to the scattering length). The thermal agitation of the nuclei, however, is responsible for some spread in the mass distribution, although as a rule the resultant "smear" of the nuclei is small compared with that of the electron clouds.

---

[8]) After Bacon, loc. cit. [3]).

The similarity between the mass distribution of the nuclei and that of the electrons, which obviously share the same periodicity in crystals, makes it clear that we can resolve the density of the nuclei into Fourier components, just as is known to be possible for the electrons. In the article cited above [1]) it was shown that these Fourier components can in fact be derived from the diffraction pattern. The structure can then in principle be determined simply by adding the components (Fourier synthesis). In *fig. 3a* and *b* an example is given of the application of this Fourier method with X-rays and neutrons, respectively.

Although this indicates that neutron diffraction and X-ray diffraction may in principle be identically treated, the quantitative difference mentioned nevertheless means that the comparison is no longer valid in some points. In the first place, where X-rays are concerned the relatively large extent of the electron cloud gives rise to considerable path differences between the rays scattered by one atom. Owing to the phase differences involved, the X-ray intensity resulting from the scattering by a single electron cloud decreases with increasing angle of deflection, and there is consequently a tendency for the reflections of increasing angle in the diffraction pattern to die out. In view of the much more concentrated distribution of the nuclear mass, no such decrease occurs with neutron diffraction. Secondly, this more concentrated distribution of the nuclear mass makes

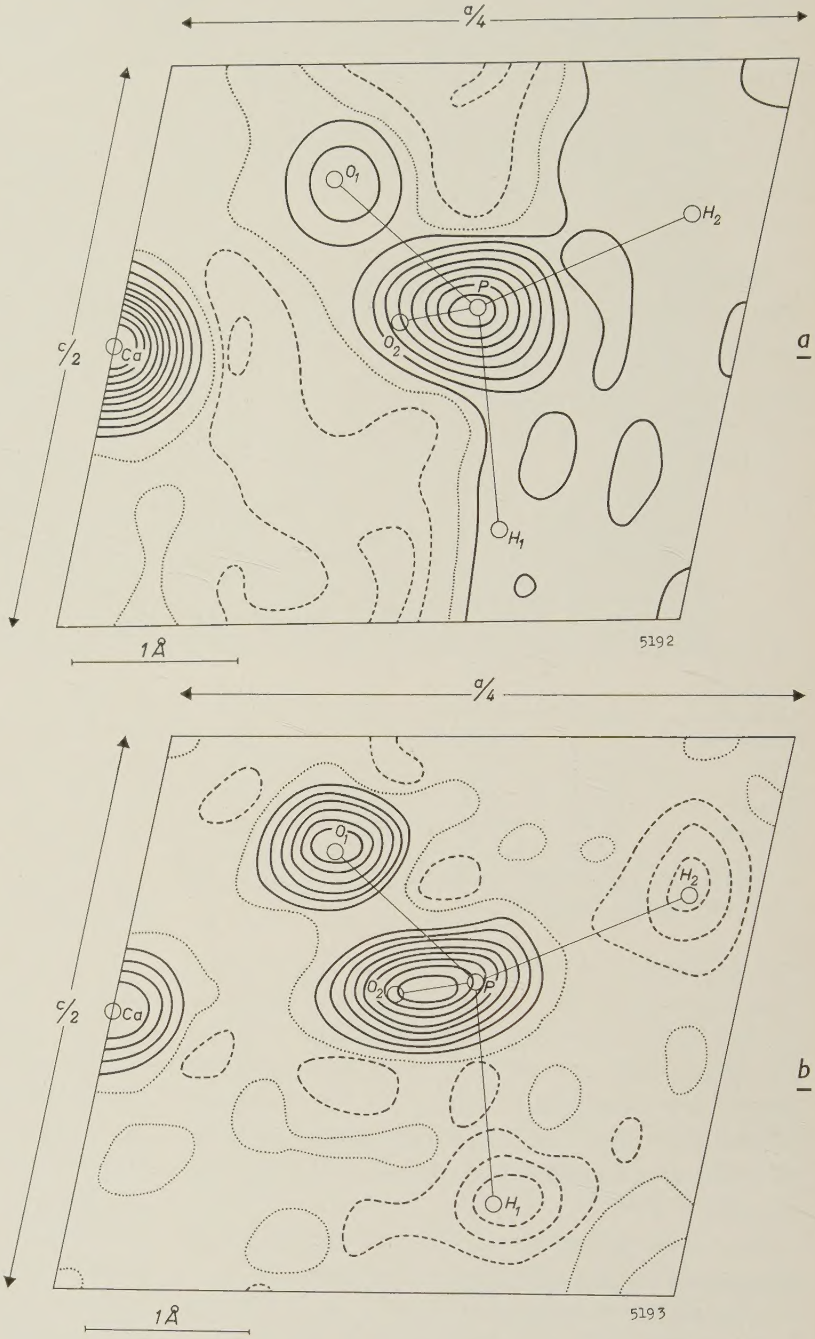

Fig. 3. Crystal structure of the compound $Ca(H_2PO_2)_2$, *a*) determined by X-ray diffraction, *b*) determined by neutron diffraction. Use was made in both cases of the Fourier method described in the article referred to under [1]). In *a*) the contours denote the distribution of the electrons, and in *b*) the distribution of the nuclei (the solid lines join places of equal positive density, the dotted lines places of zero density, and the dashed lines places of equal negative density). Note that the hydrogen atoms, of which there is no trace in *a*), are clearly visible in *b*), demonstrating one of the advantages of neutron diffraction.

The negative sign of the density at certain places in *a*) and in the "flat" parts of *b*) has no physical significance: it arises from the method of calculation adopted; for convenience a constant positive term has been omitted at all points. As regards the hydrogen atoms in *b*), however, the sign does have a physical reason, which is a phase effect involved in the scattering. For particulars see text. (After B. O. Loopstra, JENER Publications No. 15, 1958.)

the Fourier method rather unsuitable: the alternative method of "trial and error" is to be preferred.

The applicability of this much simpler method is due to the fact that neutron diffraction analysis is frequently meant to provide only supplementary information on the basis of a fairly detailed picture of the structure already provided by X-ray analysis. The object may be, for example, simply to determine the position of the hydrogen atoms, with a choice to be made between several possible positions, or to determine whether the magnetic moments present have this or that orientation. Questions such as these can be answered quite satisfactorily by the method of trial and error. This method consists in testing various crystal models by comparing the observed reflection intensities with those calculated on the basis of the models. In simple cases the method can also be used in X-ray diffraction. The calculation of the (relative) intensities of the reflections, i.e. the squares of the scattering amplitudes F, from an assumed crystal model is in itself no problem, and in the case of neutron diffraction is even somewhat simpler than in the case of X-ray diffraction. The scattering amplitudes F can be found quite simply by adding the scattering lengths of the atoms contributing to the scatter, taking into account the phase differences due to the various path differences.

Because the Fourier method is not much used in neutron diffraction analysis, we shall make no further use in this article of the representation of the above-mentioned Fourier components (density waves), on which the article cited under [1]) was based. This representation, where each reflection is regarded as produced from the fronts of a density wave, is particularly useful for elucidating the Fourier method. As regards the method of trial and error, we can base our considerations more simply on the alternative representation of individual scattering atoms, where each reflection is regarded as being produced by lattice planes.

We shall now briefly indicate how the phase differences are taken into account in the calculation of the diffraction intensities.

Suppose that atomic nuclei designated by j, having a scattering length $\mathbf{b}_j$, are situated at positions $\mathbf{r}_j$. Let S_0 and S be unit vectors in the incident and scattered directions, respectively; by adding the contributions, differing in phase, of the various atoms, we then find that the amplitude of the scattered wave must be proportional to

$$F = \sum_j \mathbf{b}_j \exp\{-2\pi \mathrm{i}\, \mathbf{r}_j \cdot (\mathrm{S}-\mathrm{S}_0)/\lambda\}. \quad . \; . \; . \quad (5)$$

A similar formula can be written for the scattering of X-radiation:

$$F = \sum_j \mathbf{c}_j \exp\{-2\pi \mathrm{i}\, \mathbf{r}_j \cdot (\mathrm{S}-\mathrm{S}_0)/\lambda\}. \quad . \; . \; . \quad (6)$$

The scattering lengths $\mathbf{c}_j$ in this equation, unlike the neutron scattering lengths, depend on the angle of deflection and the wavelength; in fact, $\mathbf{c}_j$ decreases with increasing value of $\sin \Theta/\lambda$. This naturally complicates the calculation somewhat, since for every value of $\sin \Theta/\lambda$ we must now know the corresponding value of the scattering length of each atom. The reason for this effect has already been mentioned, being the extensiveness of the electron cloud compared with the wavelength of the radiation. To give an idea of the magnitude of the decrease in question, columns 4 and 5 in Table I show the X-ray scattering lengths of the elements tabulated for $\sin \Theta/\lambda = 0$ and for $\sin \Theta/\lambda = 0.5 \times 10^8$ cm^{-1} respectively.

We shall now deal with the three examples of neutron analysis to which we have alluded, the supplementary structural data being obtained by the method of trial and error just discussed.

First example: determination of hydrogen atom sites in the alloy Th_2Al

The alloy Th_2Al can absorb gases. It may, for example, absorb hydrogen until the composition Th_2AlH_4 is reached. In the process the dimensions of the tetragonal unit cell are changed, but the relative positions of the Al and Th atoms remain unchanged. This is clearly revealed by X-ray diffraction. In Debye-Scherrer patterns of compounds having the compositions Th_2Al, Th_2AlH_2, Th_2AlH_3 and Th_2AlH_4, shown in *fig. 4*, it can be seen that the diffraction peaks are shifted, but their intensities remain virtually unchanged.

It is again quite evident from the latter fact that it is impossible to learn anything about the position of the hydrogen atoms from the X-ray scattering. There was therefore good reason to investigate these compounds with the aid of neutrons.

Since only polycrystalline samples of these compounds are available, their use in neutron diffraction involves a difficulty, especially where they contain hydrogen. In that case, in addition to *coherent* scattering, which obeys Bragg's law and with which we have been exclusively concerned in the foregoing, strong *incoherent* scattering occurs, which makes it very difficult to observe the diffraction peaks. (Incoherent scattering is discussed in the appendix to this article. Its salient feature is that, by contrast with the ideal case, there is not complete extinction of all the scattering contributions in other than the Bragg angles.)

In these investigations, therefore, deuterides were used instead of hydrides, because they give appreciably less incoherent scattering. It may safely be assumed that the deuterium atoms will occupy the same sites in the deuterides as the hydrogen atoms in the hydrides.

An incidental advantage of the use of deuterides instead of hydrides — although it scarcely makes up for the much greater difficulty of preparing the sample — is that deuterium has a greater scattering length than hydrogen, as can be seen from Table I.

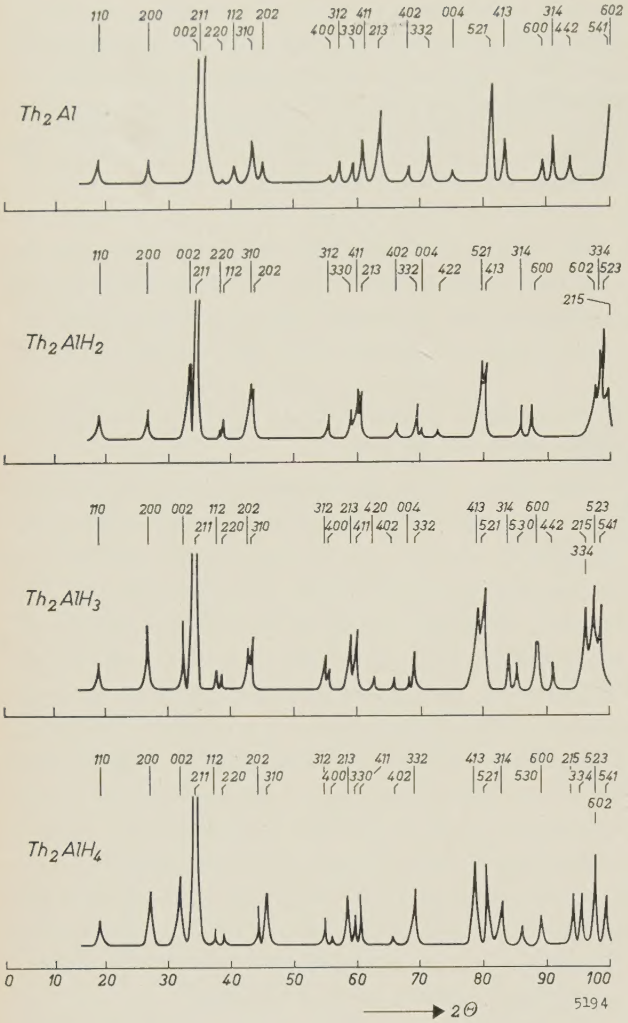

Fig. 4. Debye-Scherrer patterns of Th$_2$Al, Th$_2$AlH$_2$, Th$_2$ A/H$_3$ and Th$_2$AlH$_4$ obtained with X-rays of 1.79 Å. The intensit y is plotted versus the angle of deflection 2Θ. The Miller indices are given above the scattering curves. The diagrams differ from one another in the situation of the diffraction peaks (owing to a change in the size of the unit cell). There is little difference, however, in the intensities of the peaks, because of the small hydrogen contribution. The picture changes when neutrons are used instead of X-rays: compare these diagrams with those in fig. 5.

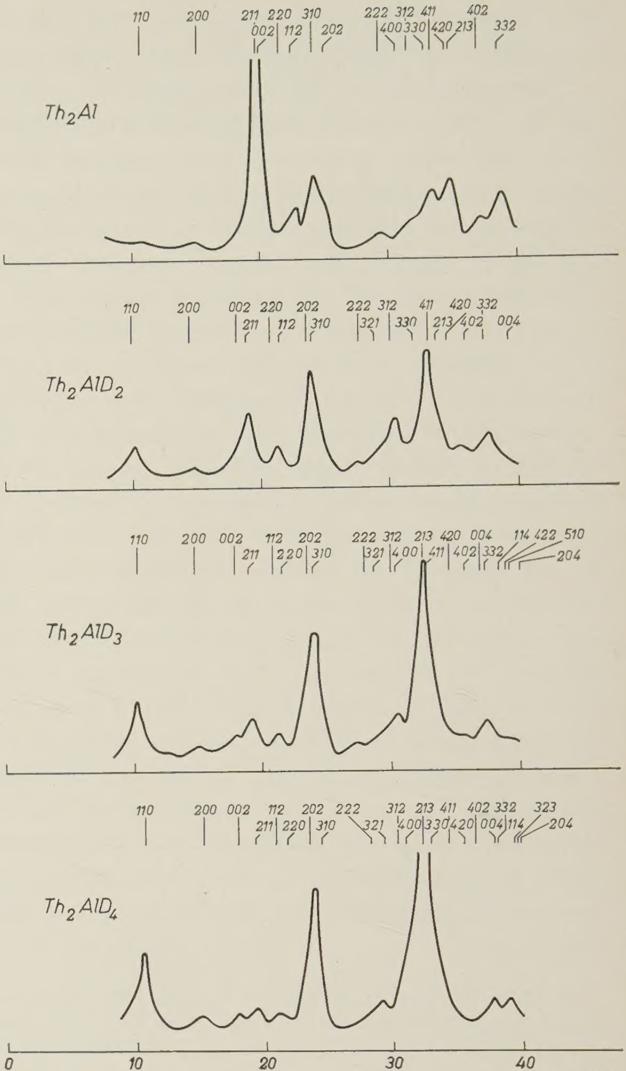

Fig. 5. Debye-Scherrer patterns of Th$_2$Al, Th$_2$AlD$_2$, Th$_2$AlD$_3$ and Th$_2$AlD$_4$ obtained with neutrons of 1.03 Å. The marked differences in the intensity of corresponding diffraction peaks demonstrate the very considerable scattering contribution made by the deuterium.

For neutron analysis [9]) samples of differing deuterium content were placed in a thin-walled tube of 1 cm diameter and mounted on the goniometer. The observed intensity, i.e. the pulse density (count rate) measured with the counter tube, was plotted as a function of the scattering angles for the various compositions in *fig. 5*.

Comparison with the X-ray diffraction patterns in fig. 4 shows practically the same succession of peaks, indicating that the substitution of deuterium for hydrogen causes no essential change in the crystal structure. The (relative) intensities of the maxima are now, however, entirely different, which is a clear illustration of the marked contribution which the deuterium makes to the scattering.

Comparison of the observed intensities with the values calculated for various models establishes the positions of the deuterium (and hence of the hydrogen) atoms in the unit cell. As assumed in [1]), they are situated in the tetrahedral interstices between the thorium atoms. There are four of these interstices for every aluminium atom, in agreement with the fact that the maximum hydrogen content achieved corresponds to the composition Th$_2$AlH$_4$. *Fig. 6* shows the unit cell of Th$_2$Al with four of these tetrahedra and the associated hydrogen atoms.

---

[9]) J. Bergsma, J. A. Goedkoop and J. H. N. van Vucht, Acta cryst. **14**, 223, 1961 (No. 3).

Neutron diffraction by magnetic atoms and ions

Neutrons possess a spin, i.e. an angular momentum, associated with a magnetic moment. This means that, contrary to what has been said above, they *can* interact with an electron cloud when the latter is the carrier of a resultant magnetic moment. The scattering then produced is in general of the same order of magnitude as that caused by the atomic nucleus, so that if a crystal contains magnetic atoms or ions, scattering due to both causes may be observed.

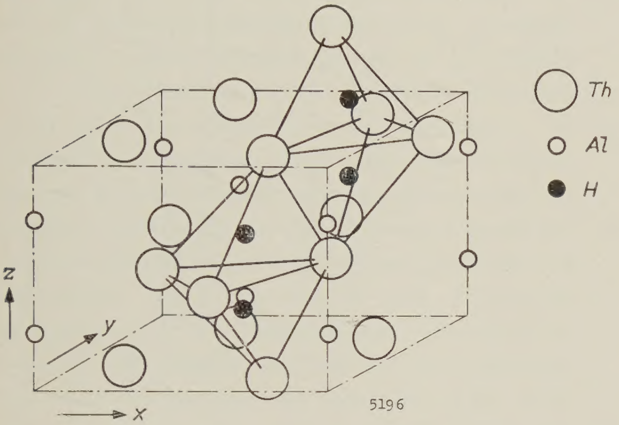

Fig. 6. The unit cell of Th_2Al. Neutron diffraction analysis shows that the gas atoms absorbed are situated in the tetrahedral interstices formed by the thorium atoms; four such tetrahedra, each with its hydrogen atom, are shown in the drawing. Where all these interstices are filled with hydrogen, the formula of the compound is Th_2AlH_4. This compound still has the same structure as Th_2Al, i.e. the thorium and aluminium atoms have the same relative positions, the change being a difference in the size of the cell.

The character of magnetic scattering depends strongly on the extent to which the magnetic moments of the atoms are in mutual alignment. If the crystal is paramagnetic, that is to say possesses no preferred orientation, the magnetic scattering is then not concentrated in diffraction peaks, as it is when due to the nuclei, but is diffuse.

Many substances are, however, only paramagnetic above a particular temperature; below this temperature the interaction between neighbouring atoms prevails over thermal agitation, so that over certain regions in the crystal (magnetized domains) all magnetic moments are oriented parallel or anti-parallel to a certain direction. Where the moments are all aligned in the same direction, the substance is said to be ferromagnetic; if some point in one direction and the others in the opposite direction, the substance is antiferromagnetic or ferrimagnetic, depending on whether the resultant moment per unit cell is zero or not. In the case of ferromagnetism and ferrimagnetism, the application of a sufficiently strong magnetic field influences the domains and brings about an externally measurable magnetization. The magnetic neutron scattering of such crystals possessing ordered magnetic moments does resemble to an appreciable extent the nuclear scattering so far considered, that is to say it is likewise concentrated in diffraction peaks according to Bragg's law. Their intensities are calculated in the same way as for nuclear scattering, except that instead of the nuclear scattering length b we must now use the quantity

$$p = 0.539 \times S\,\mathrm{f}(\sin\Theta/\lambda), \quad . \; . \; . \; . \quad (7)$$

expressed in 10^{-12} cm.

S is the effective spin-quantum number, which is a measure of the magnetic moment of the scattering atom [10] (the latter is equal to $2S$ Bohr magnetons). In antiferromagnetic and ferrimagnetic substances, S is given the positive or negative sign according to whether the moment is aligned in the one direction or the other. The other factor, $\mathrm{f}(\sin\Theta/\lambda)$, is the magnetic form factor, which is equal to unity where the reflection angle is zero, and becomes smaller as the angle decreases. The magnetic scattering of neutrons, unlike nuclear scattering, is indeed dependent on the scattering angle, and in this respect it shows more correspondence with X-ray scattering. The reason, of course, is that magnetic neutron scattering is also attributable to an electron cloud whose extent is of the order of 1 Å.

The dependence of this form factor on the scattering angle is not identical with that of the earlier introduced X-ray scattering length c, for the latter relates to the entire electron cloud around the nucleus. That cloud consists of individual shells, and the magnetic moment, if present, is attributable to the incomplete filling of one of those shells (the 3d shell, for example, in the case of Fe and Mn). It is therefore only the electrons in this shell that cause the magnetic scattering of neutrons, and consequently the magnetic form factor $\mathrm{f}(\sin\Theta/\lambda)$ is determined by the radial density distribution of those electrons alone.

In the same way as the nuclear scattering amplitude, which we shall now call F_{nucl}, was composed of the scattering lengths b of the atomic nuclei in the crystal, each multiplied by the appropriate phase factor, we can now combine the magnetic scattering lengths of the various magnetic atoms as given by equation (7) to form a magnetic amplitude, F_{magn}.

In most crystals there is no difference between the periodicity of the magnetic and the other atoms. The interference conditions are then identical for both magnetic and nuclear scattering, and therefore the observed diffraction intensities will consist of a nuclear and a magnetic part. The theory shows that the total intensity is then proportional to

---

[10] Our considerations apply to the case where the magnetic moment is entirely due to the electron spins, and not to the orbital motion of the electrons.

$$I = F^2_{\text{nucl}} + (\sin \alpha)^2\, F^2_{\text{magn}}\,, \quad . \; . \; . \quad (8)$$

where α is the angle between the preferred orientation of the magnetic moments in the crystal and the bisectrix of the angle between the incident and the scattered beams. If α is zero, the scattering is purely nuclear.

In some cases of antiferromagnetism and ferrimagnetism the magnetic moments of corresponding atoms in adjacent unit cells are oppositely oriented, and equally oriented moments are always twice as far apart. In that case there is thus indeed a difference in periodicity, the unit cell being larger in a magnetic respect than in a nuclear respect, and *extra reflections of purely magnetic origin will then occur.* The best known example of this is cubic MnO, where all edges of the unit cell are twice as long in the antiferromagnetic state [11]). It may be mentioned that neutron diffraction analysis has recently revealed cases of magnetic ordering (e.g. in metallic holmium) where neighbouring magnetic moments make angles with one another differing from 0° or 180°, giving rise to a spiral orientation [12]).

It might seem surprising that the intensities of the nuclear and magnetic scattering components are simply added together in equation (8). It might be thought that one would first have to add the amplitudes and then square their sum. This is certainly the right method if the neutrons are polarized, that is to say if the spins of the incident neutrons are artificially brought into identical alignment. The neutrons coming from the reactor are of course unpolarized, in which case the additive method gives the correct composition of the intensities. In the following we shall be concerned only with this case.

The magnetic scattering of neutrons makes it possible to determine the value of S for the various atoms in an ordered magnetic crystal, i.e. to establish the direction and magnitude of the individual atomic magnetic moments. We shall now consider two examples of this possibility, which obviously has no equivalent in X-ray diffraction.

Second example: the magnetic moments of Mn atoms in the alloy $Al_{0.89}Mn_{1.11}$ [13])

In the alloy $Al_{0.89}Mn_{1.11}$ the aluminium and manganese atoms are statistically distributed in a specific way over the two positions available for them in the tetragonal unit cell, i.e. the corner (A) and the middle (B) of the cell. It had been deduced from X-ray diffraction that the order parameter r, defined as the average fraction of Al atoms on the A sites, amounts to 0.03. This is explained in the article referred to under [1]). It is also mentioned there that the alloy can be made into a permanent magnet, so that there must be domains within which the magnetic moments of the manganese atoms are ordered. The following questions then arise:

a) In what crystallographic direction are the magnetic moments preferably oriented (in the absence of an aligning magnetic field, so that the moments are free to orient themselves)?

b) If a manganese atom occupies a B site, is its magnetic moment equally or oppositely oriented to that of the manganese atoms on most of the surrounding A sites? In other words, is the coupling between these neighbours ferromagnetic or ferrimagnetic? The results of X-ray diffraction analysis and measurement of the saturation magnetization of samples treated in different ways have prompted the supposition that this coupling is ferrimagnetic.

c) How large is the magnetic moment of each Mn atom?

The answers to these questions are to be found from the Debye-Scherrer pattern in *fig. 7*, obtained by neutron diffraction. The intensities derived from the peaks by planimetry are given in the last column of *Table II.*

Both in the figure and in the table the diffraction peaks are characterized by the Miller indices h, k

Table II. Observed and calculated intensities of neutron reflections from polycrystalline $Al_{0.89}Mn_{1.11}$.

Miller indices *hkl*	Magnetic angle factor $(\sin \alpha)^2$	Magnetic form factor $f(\sin \Theta/\lambda)$	Calculated intensities				Observed intensities *)
			nuclear contribution	magnetic contribution	total		
001	0.00	—	6.56	0.00		6.56	6.70±0.12
100	1.00	0.68	8.00	3.59		11.59	11.66±0.11
101	0.62	0.54	0.22	0.98		1.20	1.32±0.08
110	1.00	0.45	0.09	0.44		0.53	0.73±0.07
002	0.00	—	0.03	0.00	0.03 }	6.68	6.47±0.12
111	0.77	0.34	6.12	0.53	6.65 }		
102	0.29	0.28	4.61	0.10		4.71	4.52±0.10
200	1.00	0.20	0.05	0.05		0.10	0.12±0.06
112	0.45	0.19	0.08	0.03	0.11 }	7.79	8.20±0.19
201	0.86	0.18	3.45	0.10	3.55 }		
210	1.00	0.15	3.18	0.07	3.25 }		
003	0.00	—	0.73	0.00	0.73 }		
211	0.89	0.11	0.12	0.03	0.15 }		
202	—	—	0.05	—	0.05 }	0.11	0.14±0.08
103	—	—	0.05	—	0.05 }		
212	—	—	4.33	—	4.33 }	6.48	6.26±0.12
113	—	—	2.15	—	2.15 }		

*) The limits of error indicated in this column relate only to the probable statistical error in counting the number of neutrons.

---

[11]) C. G. Shull and J. S. Smart, Phys. Rev. 76, 1256, 1949.

[12]) Personal communication from W. C. Koehler.

[13]) P. B. Braun and J. A. Goedkoop, to be published in Acta cryst.

and l, whose significance we shall briefly recall. Let a, b and c be the edges of the unit cell (a parallelepiped), then two successive lattice planes with Miller indices h, k and l cut from the three edges respectively the portions a/h, b/k and c/l. The unit cell is here tetragonal; $c = 3.54$ Å is the tetragonal axis; the axes $a = b = 2.77$ Å are perpendicular thereto.

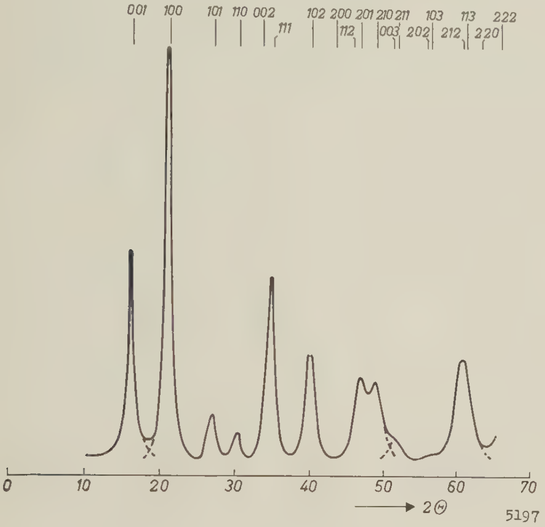

Fig. 7. Debye-Scherrer patterns of the alloy $Al_{0\cdot 89}Mn_{1\cdot 11}$ with neutrons of 1.03 Å. At large deflection angle 2Θ the intensities are almost entirely determined by nuclear scattering. They are weak where $h + k + l$ is even, and strong where $h + k + l$ is odd. This is due to the preference shown by the manganese and aluminium atoms for the corners and centre, respectively, of the tetragonal unit cell, and to the opposite sign of the scattering lengths of these atoms, see Table I. (In X-ray diffraction, where there is no such difference in sign, the reflections are strong where $h + k + l$ is even, and weak where $h + k + l$ is odd, i.e. the situation is the reverse of that in neutron diffraction.) The reflections 100, 101 and 110, but not 001, comprise an appreciable magnetic contribution in addition to that due to the nuclei.

Regarding the calculation of the intensity of the reflections, only two cases are to be distinguished here, namely reflections corresponding to lattice planes where $h + k + l$ is even and where $h + k + l$ is odd; for brevity we shall refer to them as even and odd reflections. It is easily seen that, if the A site lies in a lattice plane of a particular set, the B site for an even reflection will also lie in a lattice plane of the same set, but for an odd reflection it will lie midway between the lattice planes of that set. Thus, for even reflections the scattering contributions of A and B positions must be added, whereas for odd reflections it is necessary to take the difference.

In analysing the diffraction pattern we begin with large scattering angles, for it is here, owing to the decrease in magnetic scattering already discussed, that the intensities are almost entirely of nuclear origin. As with X-ray diffraction, the measured scattering intensities are compared with the intensities calculated for different values of the order parameter r. The best agreement was found for $r = 0.03$, which agrees within the accuracy of the measurement with the value found by X-ray diffraction. The corresponding distribution of the Al and Mn atoms over the corners and centres of the unit cell is represented in *fig. 8*.

We can now calculate the nuclear contributions of all intensities, including those at small scattering angles. The relevant values are given in the fourth column of Table II.

Comparison of these with the measured intensities makes it clear that there must still be appreciable magnetic contributions at small scattering angles. Let us assume for a moment that the magnetic moments of Mn atoms on A and B sites are in parallel orientation. At the value found for r the A sites will be occupied by an average of 0.97 Mn atoms, and therefore, in view of the total composition, there will be 0.14 on B sites. For even reflections we must add the scattering contributions; the scattering amplitude per unit cell is thus:

$$F_{\mathrm{magn}} = 1.11\,p \quad (\text{with} \quad h + k + l \quad \text{even}),$$

where p is the magnetic scattering length per Mn atom, to be calculated from eq. (7). For odd reflections (still with the two magnetic moments parallel) we must subtract one scattering contribution from the other, giving

$$F_{\mathrm{magn}} = 0.83\,p \quad (\text{with} \quad h + k + l \quad \text{odd}).$$

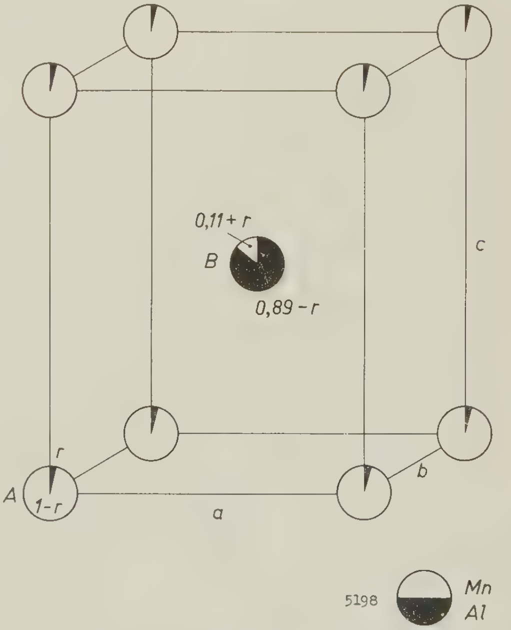

Fig. 8. The distribution of the aluminium and manganese atoms over the corners and centres of the unit cell of the compound $Al_{0\cdot 89}Mn_{1\cdot 11}$. The average fraction r of the aluminium atoms at the corners, here represented as a sector of a circle, is roughly 0.03, as found by both X-ray and neutron diffraction.

If, on the other hand, the moments on A and B sites are oppositely oriented, then according to the remarks concerning equation (7) the contribution of the B sites must be given the negative sign so that the two above equations must be interchanged.

As may be seen from Table II, the observed intensity for the first reflection (001) can be explained within the limits of experimental error by the nuclear contribution alone. It follows from the foregoing that F_{magn} cannot be zero, so we must assume that α in eq. (8) is zero for this reflection.

The Miller indices indicate that this reflection depends on lattice planes perpendicular to the tetragonal c axis. Since α is the angle between the perpendicular to the lattice planes and the preferred direction of the magnetic moments in the crystal, it may therefore be concluded that the magnetic moments must be oriented along the c axis, which answers question (*a*).

Armed with this knowledge, we can calculate $(\sin\alpha)^2$ from equation (8) for the other reflections: the results are given in the second column of Table II. The third column contains the values of the magnetic form factor $f(\sin\Theta/\lambda)$, taken from the results of the neutron analysis of other manganese compounds.

Using these data in conjunction with equations (7) and (8), the value of the effective spin-quantum number S (see eq. (7)) giving the best agreement with the observed intensities was now calculated for the three reflections with the greatest magnetic contribution (100, 101, 111), in respect of the two possible mutual orientations of the spins on A and B sites. It was found that in the case of antiparallel orientation the three S values thus obtained were in better agreement with one another than in the case of parallel orientation. It was inferred from this that the spins are oppositely oriented, which disposes of question (*b*): as has already been assumed, the coupling is ferrimagnetic. The value of S thus found was 0.97, so the magnetic moment of the Mn atoms is 1.94 Bohr magnetons, which answers question (*c*).

The fifth column of Table II gives the magnetic contributions to the intensities, calculated for this model; the sum of nuclear and magnetic contributions in the sixth column is now seen to be in good agreement with the measured values. Further confirmation is that the saturation magnetization calculated for this structure is in quantitative agreement with the experimental value.

Third example: the magnetic structure of $Y\text{-}Ba_2Zn_2Fe^{III}{}_{12}O_{22}$

Our second example of magnetic structure analysis concerns $Y\text{-}Ba_2Zn_2Fe^{III}{}_{12}O_{22}$ (Y denotes the type of structure). In this case a single crystal was available, without which the neutron analysis of such an intricate compound would not have been easily possible. This structure was also discussed in the above-mentioned article [1]: the unit cell is hexagonal, with a very long c axis (43.6 Å), and contains 36 iron atoms, all of which have a magnetic moment. From magnetic measurements the substance is known to be ferrimagnetic and belongs to the class described as "ferroxplana", in which the magnetic moments are oriented perpendicular to the c axis. On theoretical grounds, Gorter [14] had already drawn up a model of the magnetic structure, which is shown in *fig. 9*.

The primary object of the neutron analysis [15] was to verify this model. It was done by measuring the intensities of 18 reflections from lattice planes perpendicular to the c axis (003, 006, . . . , $00\overset{\frown}{54}$; the intermediate reflexions are "forbidden" on grounds of symmetry). Since the magnetic moments are also perpendicular to the c axis, the angle α of equation (8) is always 90° for such reflections, so that the magnetic scattering makes the maximum possible contribution.

Experimentally it is a very simple matter to measure such a series of intensities, because the reflections all lie in one plane. The crystal needs to be aligned only once, with the c axis in the appropriate (horizontal) direction, after which all reflections are successively recorded with one sweep of the counter tube.

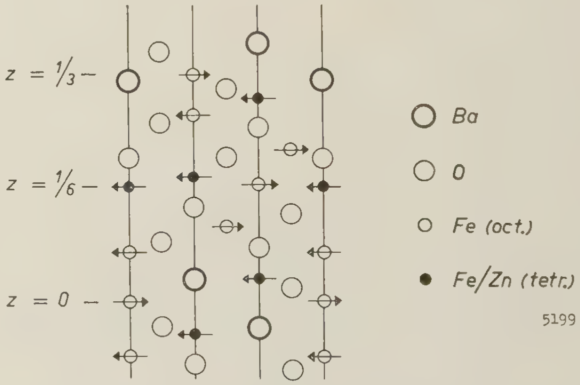

Fig. 9. The magnetic structure of $Y\text{-}Ba_2Zn_2Fe_{12}O_{22}$, as proposed by Gorter [14] and confirmed by neutron diffraction. The figure represents a cross-section along the (110) plane; the z coordinate is expressed as a fraction of the lattice constant c. The directions of the magnetic moments of the iron atoms, which are all perpendicular to the hexagonal crystal axis, are indicated by arrows.

---

[14] E. W. Gorter, Proc. Instn. Electr. Engrs. **104 B**, suppl. No. 5, 255, 1957.

[15] J. A. Goedkoop, J. Hvoslef and M. Živadinović, Acta cryst. **12**, 476, 1959.

The intensities found were then compared with the sum of the nuclear intensities (calculated from Braun's model[16]) and the magnetic intensities (from Gorter's model[14]). The results were in good agreement with the theory, so that this relatively simple measurement may be regarded as a confirmation of the postulated magnetic structure. Moreover, as regards the nuclear contribution, Braun's conclusion was again confirmed, namely that the zinc atoms together with an identical number of iron atoms are distributed at random over two different crystallographic positions. As appears from the neutron and X-ray scattering lengths of Zn and Fe, given in Table I, the neutron intensities are more sensitive in this particular point than the X-ray intensities.

As the intensity (in photons per cm^2 per second) of a given X-ray tube is still greater by several powers of ten than the neutron flux of the largest nuclear reactors, and in view of the comparative scarcity of nuclear reactors, neutron diffraction is at present used as a supplementary method for answering those questions that cannot readily, if at all, be answered by means of X-ray diffraction. Neutron analysis, then, is always preceded by X-ray analysis. In this connection, close cooperation is desirable between the research centres where nuclear reactors are available and the laboratories where the most diverse structural problems are frequently dealt with. The three examples presented in this article may serve as an illustration of such cooperation.

Appendix: Incoherent scattering

Coherent scattering, with which we have been primarily concerned, is found when the atoms at identical lattice sites in the crystal all contribute to the scattering with identical scattering lengths. *Incoherent scattering* occurs where they do not all contribute with the same scattering length. In that case it is readily seen that there is no longer complete extinction of all the scattering contributions in other than the Bragg angles. The phenomenon is observable in the scattering from an isotope mixture, for example. We shall take this example to illustrate the method of calculating the coherent and incoherent components of the scattering, after which we shall return to the case dealt with in the text (p. 75).

Suppose that on identical lattice sites there are n atoms of scattering length b_1 and m atoms of scattering length b_2. This is to a first approximation equivalent to *identical* scatterers on all the lattice sites in question, with a scattering length equal to the weighted mean:

$$b_{\rm H} = \frac{n}{n+m}\, b_1 + \frac{m}{n+m}\, b_2 . \quad . \; . \; . \quad (9)$$

(The index H refers to the example on p. 75.)

These identical scatterers give rise to a diffraction pattern consisting of discrete peaks; their scattering length $b_{\rm H}$ is called the *coherent scattering length.* There still remains, however, a residual component of scattering power on each of the sites in question: on the n sites with a scattering length of:

$$b_1 - b_{\rm H} = \frac{m}{n+m}\,(b_1 - b_2)\,,$$

and on the m sites:

$$b_2 - b_{\rm H} = \frac{n}{n+m}\,(b_2 - b_1)\,.$$

These "residues", which are distributed at random over the available lattice sites, give rise to a continuous diffraction pattern. As a result of this random distribution, each "residue" can be considered independent of the other, and an effective scattering cross-section can be ascribed to each (see p. 73). We can now calculate the weighted mean of these; this is known as the *effective cross-section for incoherent scattering*:

$$\sigma_{\rm H,inc} = 4\pi \left[\frac{n}{n+m}\,(b_1 - b_{\rm H})^2 + \frac{m}{n+m}(b_2 - b_{\rm H})^2\right] = $$

$$= 4\pi \left[\frac{nm}{(n+m)^2}\,(b_1 - b_2)^2\right] . \quad . \; . \; . \quad (10)$$

We also introduce an *effective cross-section for coherent scattering*:

$$\sigma_{\rm H,coh} = 4\pi b_{\rm H}{}^2 . \quad . \; . \; . \; . \; . \; . \; . \quad (11)$$

Finally we may define an *effective cross-section for the total scattering*, being the sum of (10) and (11):

$$\sigma_{\rm H,tot} = 4\pi \left[\frac{n}{n+m}\, b_1{}^2 + \frac{m}{n+m}\, b_2{}^2\right] . \quad . \quad (12)$$

Since only the coherent scattering can tell us anything about the structure of a substance, we can only determine the structure of those substances in which the effective cross-section for incoherent scattering is not unduly large compared with that for coherent scattering.

Let us now return to the hydrides of Th$_2$Al, mentioned in the text. The incoherent neutron scattering here arises from the fact that both the neutron and the scattering proton have a spin of $\frac{1}{2}$. There are consequently two possible modes of scattering, i.e. with the spins of the particles parallel or antiparallel. The total spin of the system proton plus neutron is equal to 1 in parallel orientation and equal to 0 in antiparallel orientation, which means that the probability of the former is three times greater than of the latter (this has been explained elsewhere[3]). In the case of neutron scattering by a crystal containing hydrogen, this implies that in three-quarters of the encounters the spins of neutron and proton will be parallel and in one-quarter antiparallel.

The scattering lengths in the two cases differ considerably, and are denoted by b_1 and b_2 respectively:

$$b_1 = +1.04 \times 10^{-12}\ {\rm cm}; \quad b_2 = -4.7 \times 10^{-12}\ {\rm cm}.$$

Using equations (9), (10) and (11) we calculate that $\sigma_{\rm H,coh} = 1.8 \times 10^{-24}$ cm^2 and that $\sigma_{\rm H,inc} = 79 \times 10^{-24}$ cm^2.

The difficulty mentioned in the text is now clear: of the scattering caused by the hydrogen atoms, which is in itself very considerable, only a little more than 2% contributes to the interference peaks; the remainder produces isotropic scatter, which appears as a continuous background in the diffraction patterns. This is particularly serious where polycrystalline samples are concerned, since in their case only a small proportion of the crystallites takes part in the interference peaks, although the whole sample contributes to the incoherent scattering. In a single crystal the situation is much more favourable, and hydrogen diffraction does appear in the patterns.

---

[16] See P. B. Braun, Philips Res. Repts **12**, 491, 1957, and G. H. Jonker, H. P. J. Wijn and P. B. Braun, Philips tech. Rev. **18**, 145, 1956/57.

The effect discussed here in connection with hydrogen also occurs in cases of scattering by other nuclei that have a spin differing from zero. In vanadium, for example, coherent scattering is practically imperceptible for this reason. In deuterium, having a nuclear spin of 1, we find $\sigma_{\mathrm{D,inc}} = 2.0 \times 10^{-24}\ \mathrm{cm}^2$, $\sigma_{\mathrm{D,coh}} = 5.4 \times 10^{-24}\ \mathrm{cm}^2$, indicating that most of the scattering here is certainly capable of interference.

Summary. By collimating and selecting neutrons extracted from a nuclear reactor through a channel in the shield, a monochromatic beam is obtained (i.e. one containing neutrons of one specific velocity). A sample to be analysed is placed in this beam, and the scattering intensity in various directions is measured with a counter tube filled with BF_3. Methods analogous to those in X-ray diffraction are then used to draw conclusions regarding the crystal structure from the recorded diffraction pattern. Points where neutron diffraction corresponds to and differs from X-ray diffraction are discussed in this article. In general the scattering is caused by atomic nuclei, but in special cases it is due to the electrons, i.e. when the latter are carriers of a resultant magnetic moment. Neutron diffraction is particularly used for *a*) localizing hydrogen atoms; *b*) distinguishing between atoms having consecutive atomic numbers and which are therefore difficult to distinguish by X-ray diffraction; *c*) determining the orientation of magnetic moments. An example of each of these cases is discussed (the preparatory X-ray work for these examples has earlier been described in this journal). Among the results achieved with neutron diffraction has been the determination of the complicated magnetic structure of the compound $\mathrm{Y\text{-}Ba_2Zn_2Fe^{III}{}_{12}O_{22}}$, which has served to confirm the theoretical model proposed by Gorter.

PROJECTION TOPOGRAPHS OF DISLOCATIONS

by A. E. JENKINSON *).

548.4:778.33

Dislocations have become a tangible reality for the research worker since methods were devised for making them visible, either indirectly by "decoration" or directly with the aid of the electron microscope. X-ray diffraction is the basis of yet another elegant method for photographing and studying dislocations.

About three years ago, an elegant method was devised by A. R. Lang for making visible the dislocations present in thin slices of single crystals 1). This method, which is based on X-ray diffraction, may be understood by reference to *fig. 1*.

A collimated beam of penetrating X-rays, e.g. MoKα or AgKα radiation, impinges on the crystal under study and is reflected according to the Bragg condition from an appropriate set of lattice planes, oriented preferably normal or nearly normal to the surface of the crystal slice. A suitable aperture in a screen behind the crystal allows the transmitted reflected beam to fall on a film, while the direct beam is intercepted. A diffraction image is produced on the film, representing a picture of the part of the crystal lattice traversed by the direct beam. The images of all points lying along one line in the direction of reflection coincide on the film. The topography within the crystal is thus pictured as seen in this particular projection.

If a sufficiently wide beam of almost parallel X-rays were available, a projection picture of the whole crystal could be produced with this simple set-up. Such a beam is however impracticable. Nevertheless a picture of the complete crystal can be obtained by mounting the crystal and the film on an accurately machined slide and moving them together in a certain direction, e.g. parallel to the crystal slice, while the primary X-ray beam and the screen are stationary. The Bragg condition is, of course, not affected by such a purely translational movement, and the topographical relation-

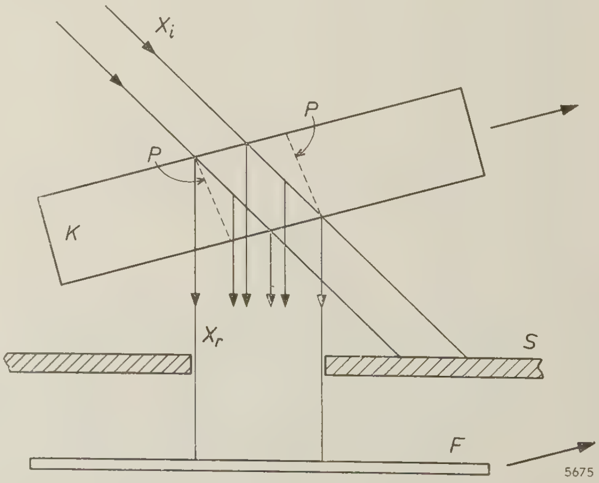

Fig. 1. Principle of projection topography as devised by A. R. Lang 1). *K* slice of a single crystal. X_i incident X-ray beam. X_r diffracted X-rays. *P* lattice planes in Bragg reflection position. *F* film. *S* screen with aperture. Crystal and film are mounted on a slide and moved together during exposure in the direction of the heavy arrows.

---

*) Mullard Research Laboratories, Salfords, England.

1) A. R. Lang, The projection topograph: a new method in X-ray diffraction microradiography, Acta cryst. **12**, 249-250, 1959.

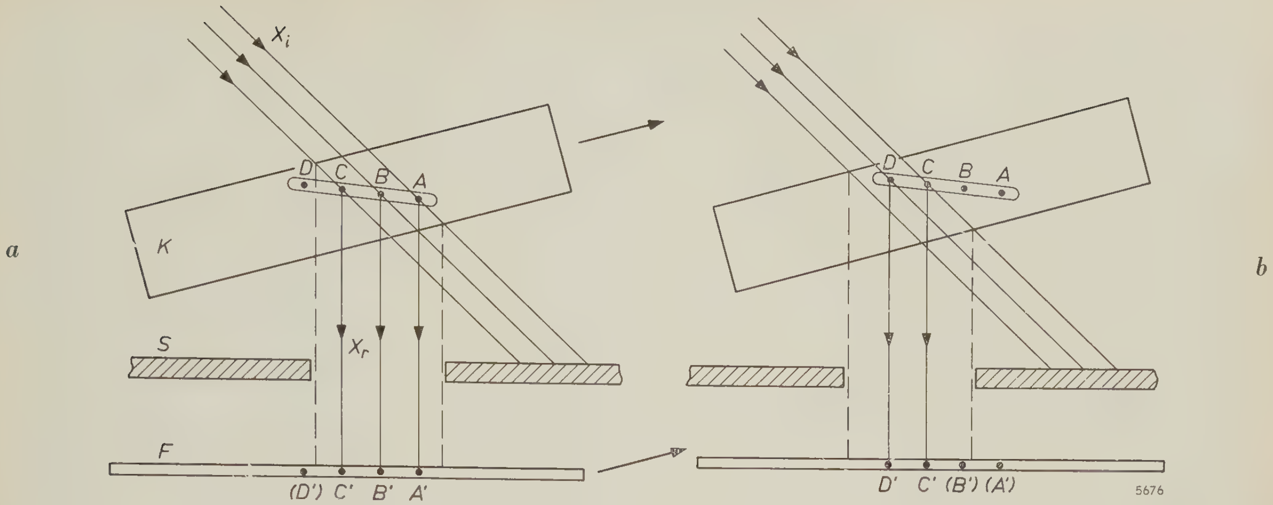

Fig. 2. Topographical details *ABCD* of an imperfection within the crystal are projected on to the film along the direction of X-ray reflection. In successive positions (*a*) and (*b*) of the crystal, each point within it, e.g. *C*, is always imaged in the same point of the film.

ship between crystal and film is obviously preserved in the overlapping diffraction images produced in successive positions (*fig. 2*). The entire crystal can be "scanned" in this way, much as a television picture is scanned (except that in the present case a ribbon-shaped scanning beam is used — see below — and a one-dimensional sweep is therefore sufficient).

An ideal crystal, having equal "reflectivity" in all parts, will give rise to a rather monotonous "picture", viz, a uniform blackening of the film. Any imperfections that disturb the lattice periodicity, however, such as dislocations, low-angle grain boundaries, etc., are found to reflect *more* than the perfect lattice surrounding them and therefore to produce an image of enhanced density on the film 2). Thus a dislocation, which in this context can be regarded as a tubular region of relatively imperfect crystal set in a matrix of perfect crystal, will produce a line on the film representing the projection of the dislocation along the diffracted beam, as shown in fig. 2.

In *fig. 3* a "projection topograph" obtained in this way is reproduced. It shows part of a slice

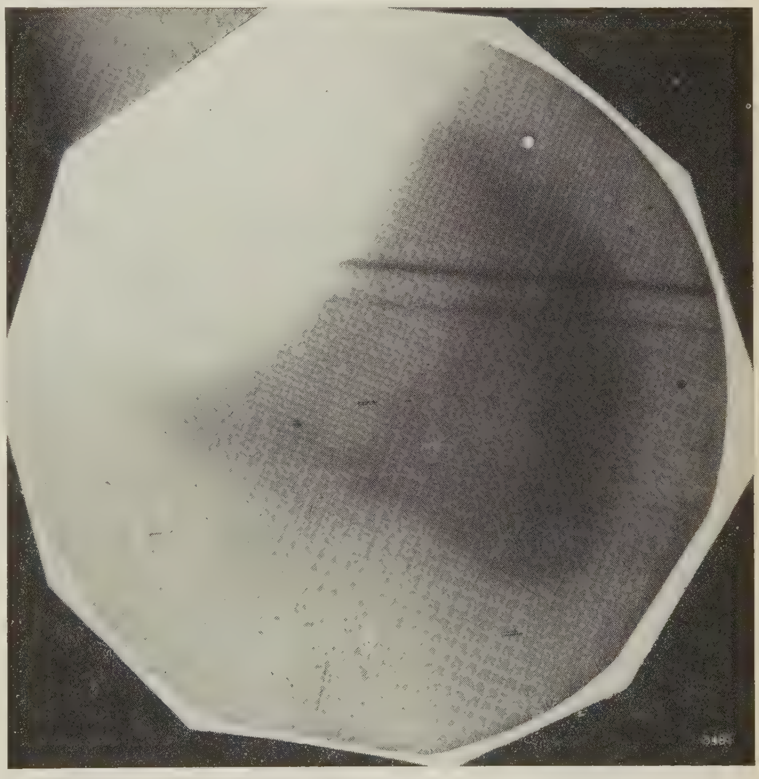

Fig. 3. Projection topograph of a germanium crystal slice about 0.1 mm thick. The total exposure time was 60 hours.

Part of the scanned crystal has produced no picture because the very thin slice had been bent in the process of mounting. The two dark bands crossing the picture are due to a spurious reflection. Other diffuse periodic lines in the picture occur because of some regular mechanical characteristic of the traverse unit. The central dark area represents a variation in the crystal thickness which is characteristic of an enhanced etching rate often found in dislocation-free Ge crystals (see A. G. Tweet, J. appl. Phys. **30**, 2002-2010, 1959). The "fringes" visible around this region and at the periphery of the crystal are due to a type of interference phenomena occurring at wedge-shaped specimens ("Pendellösung", see N. Kato and A. R. Lang, Acta cryst. **12**, 787-794, 1959).

---

2) This effect, which is not yet fully understood theoretically, is only shown by *thin* crystal slices, the criterion being $\mu d \leq 1$, where μ is the absorption coefficient and d the thickness of the slice. With a large crystal, e.g. $\mu d \approx 10$, the effect is replaced by the earlier known phenomenon of anomalous transmission (see e.g. L. P. Hunter, J. appl. Phys. **30**, 874, 1959), which entails a *decrease* in intensity of both the direct beam and the reflected beam as a consequence of imperfections.

about 0.1 mm thick of a germanium crystal rather free of dislocations [3]. The total exposure time was 60 hours.

Part of the scanned portion of the crystal slice has produced no picture. This is because the crystal has been bent in the mounting to such a degree that the relevant lattice plane was here no longer in the Bragg reflecting position. A bend with a radius of curvature of *1 mile* would be sufficient to produce this effect.

In actual practice, the crystal and film are made to perform many traverses during one exposure, instead of just one single scan. The reason is that the exposure is more easily controlled by varying the number of traverses than by changing the rate of scanning. Moreover, possible fluctuations of the X-ray intensity are rendered harmless in this way. For the very long exposure of 60 hours for fig. 3, the scanning beam made 80 traverses about 1″ long.

The apparatus for taking the projection topographs, together with the scanning mechanism, is shown in *fig. 4*.

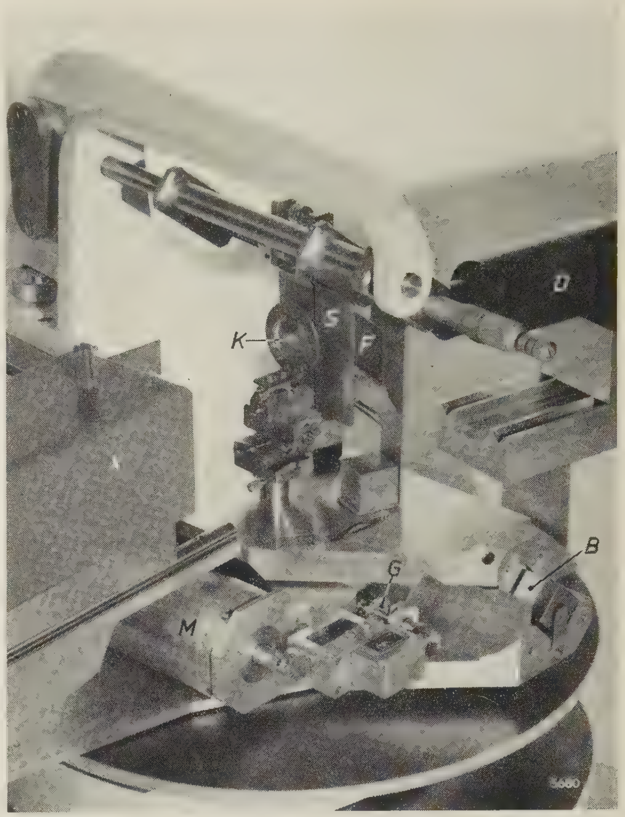

Fig. 4. Apparatus as devised by Lang [1] for making X-ray-diffraction projection topographs. *M* electric motor for scanning. *G* gears driving micrometer screw for scanning. *B* accurately machined guide bar on which the slide carrying crystal slice and film moves. *X* collimating slit. *D* detector for setting apparatus. Other letters as in fig. 1.

The motor *M* is a synchro (magslip) driven from a control unit (not shown) in which the range of the to-and-fro movement can be pre-set.

A few more remarks on the scanning method should be made. The divergence of the X-ray beam in a plane perpendicular to that of fig. 1, i.e. to the plane of the incident and diffracted beams (transverse divergence) will not affect the resolution of the picture as long as the effective focus width is small enough [4]. A transverse divergence of 3° is used in practice, allowing a crystal 1″ wide to be scanned. The divergence *in* the plane of fig. 1 (longitudinal divergence), on the contrary, is strictly limited. The criterion is that the angular spread of the incident rays should be less than the difference in Bragg angles of the Kα_1 and Kα_2 components of the X-radiation used. In this way the α_1 component alone is selected to produce the topograph, and superimposition of images due to the α_1 and α_2 components is avoided. On the other hand, the longitudinal divergence should be large enough to cover completely the natural spread of reflection due to the imperfections under study. A suitable value is $1\frac{1}{2}'$.

The primary beam at the crystal is thus ribbon-shaped and has a cross-section of 1″ × 0.005″. It is obtained by suitable collimating slits [5].

In regard to the scanning direction, it may be noted that a motion parallel to the film instead of parallel to the crystal slice would also be possible. In fact this would allow the smallest possible distance between crystal and film. Such a motion, however, would entail a displacement of the reflected beam as the crystal traverses the fixed primary beam, and it would therefore necessitate a relatively wide screen aperture, whereas in practice this aperture should be as small as possible in order to reduce the adverse effect of scattered radiation. The larger crystal-film distance necessary with the motion as shown in fig. 1 causes only a very slight increase of the geometric unsharpness.

With silicon the dislocation density is usually much higher than in the germanium crystal studied in fig. 3. See *fig. 5*, a topograph of a ½-mm slice of a silicon crystal prepared by the "floating-zone" technique [6]. As may be seen from this figure, even in a thin slice of a silicon crystal the number of dislocations revealed by a projection topograph may be so large that it is difficult to visualize the actual situation of dislocations in the crowded environment and to interpret their distribution correctly. A further refinement of the method — also introduced by Lang — provides for this by producing *stereo* pictures. After one projection topograph has been completed, the crystal slice is rotated through twice

---

[3] The crystal was provided by B. Okkerse of Philips Research Laboratories, Eindhoven. See: B. Okkerse, A method of growing dislocation-free germanium crystals, Philips tech. Rev. **21**, 340-345, 1959/60.

[4] A microfocus X-ray generator such as has been developed for X-ray microradiography, with effective focus dimensions of about 100 × 100μ is very suitable (e.g., the Hilger microfocus unit with the line focus viewed almost end-on).

[5] On the geometric considerations, see also A. R. Lang, Acta metall. **5**, 358, 1957, especially pp. 360/361.

[6] See e.g. J. Goorissen, Philips tech. Rev. **21**, 185, 1959/60.

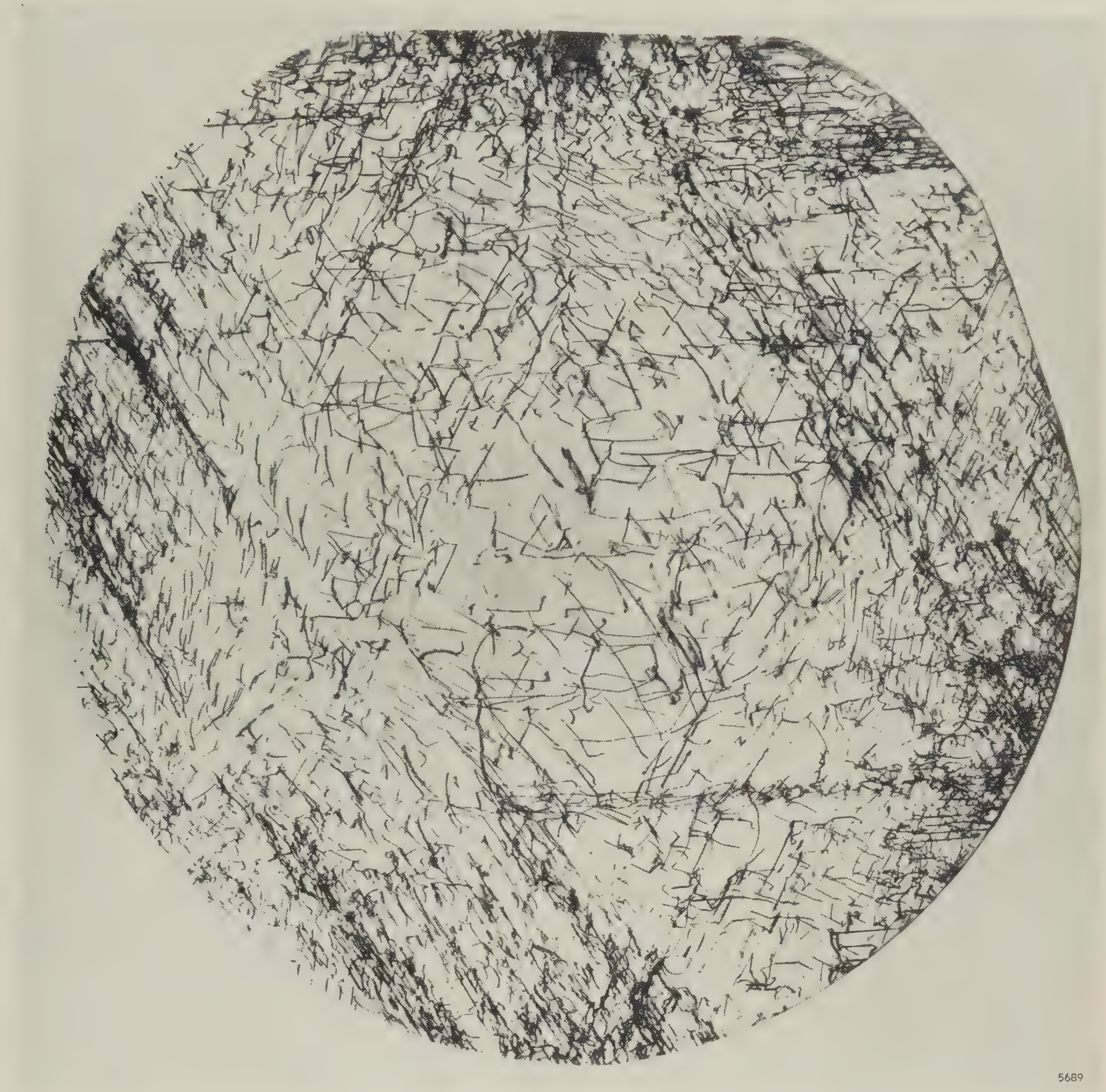

Fig. 5. Projection topograph of a $\frac{1}{2}$-mm slice of a single crystal of silicon, cut from a single crystal prepared by the "floating-zone" technique. Total exposure time 20 hours. Reflection from the $(02\bar{2})$ plane was used, with Bragg angle $\Theta \approx 16°$.

the Bragg angle, as shown in *fig. 6*, and a second projection topograph is made in this position. (This amounts to using the Bragg reflection of index $(\bar{h}\,\bar{k}\,\bar{l})$ if in the first topograph the $(h\,k\,l)$ reflection was used.) This will result in a different projection on

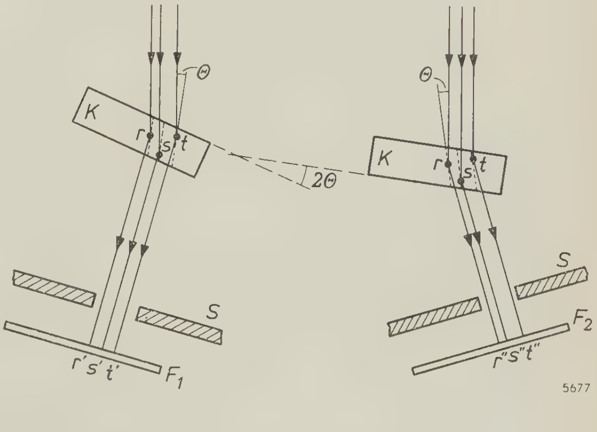

Fig. 6. A stereo pair of pictures F_1-F_2 is obtained by turning the crystal slice through twice the Bragg angle Θ as shown. Topographical details *rst* are pictured in points $r's't'$ of F_1 and in points $r''s''t''$ of F_2.

Other methods of rotation for obtaining stereo pairs are possible, but they would involve remounting of the crystal, which is a tedious procedure, especially because of the danger of bending (cf. fig. 3).

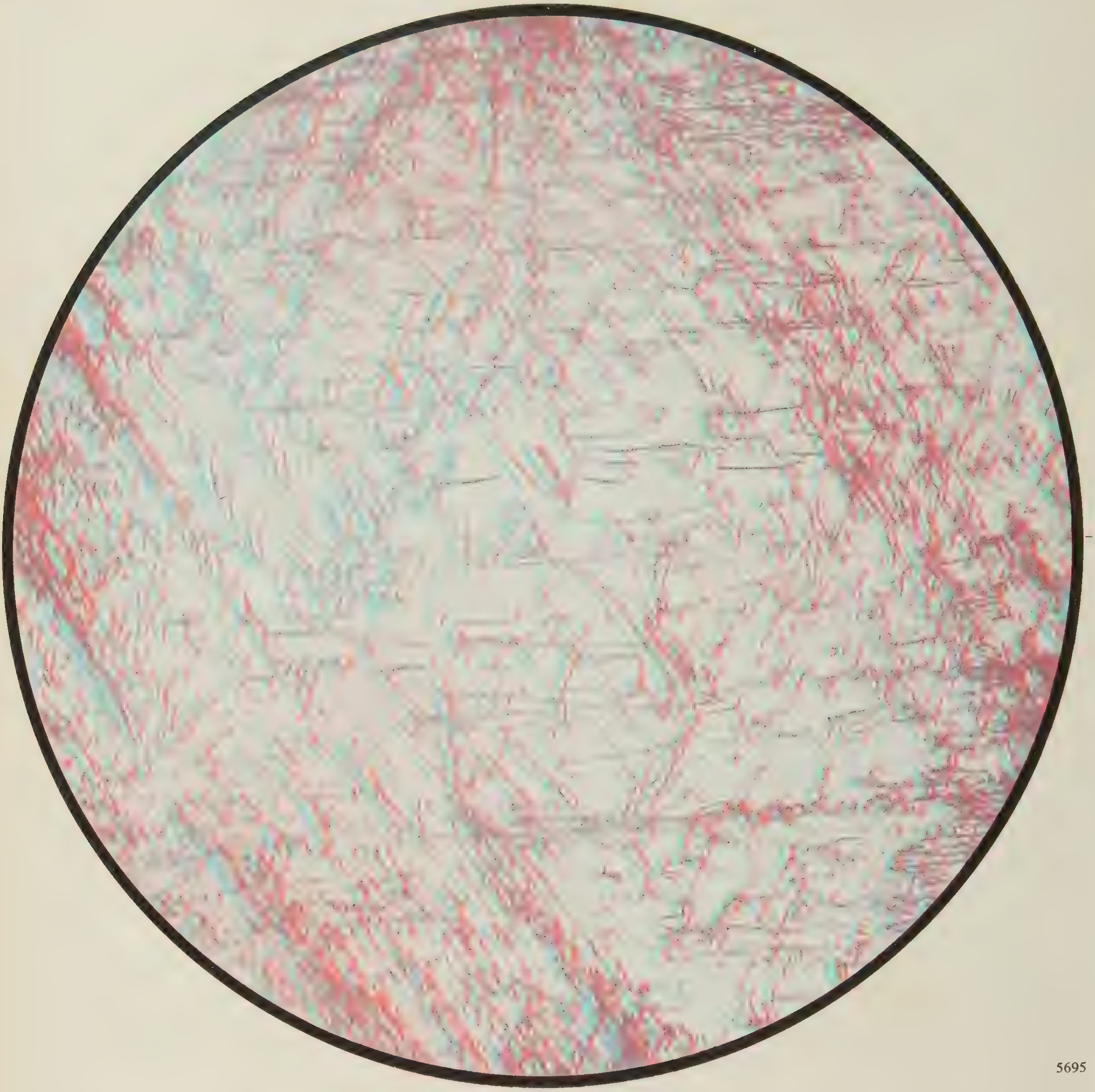

Fig. 7. Anaglyph of a stereo pair of projection topographs of silicon (cf. fig. 5). This figure should be viewed through the red-blue spectacles provided (red on the left). Most of the dislocations visible here as short pointed lines extending through the whole thickness of the slice are "60° dislocations" produced by plastic deformation. Many of the long lines lying in a plane parallel to the photograph, i.e. in what was at one time a solid-liquid interface, are screw dislocations. In this portion several examples of dislocation climb (spirals) and dislocation interaction (step-lines) are evident.

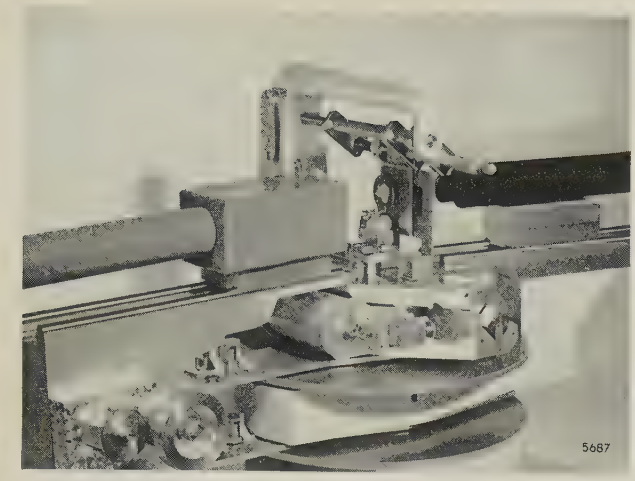

Fig. 4 *A*

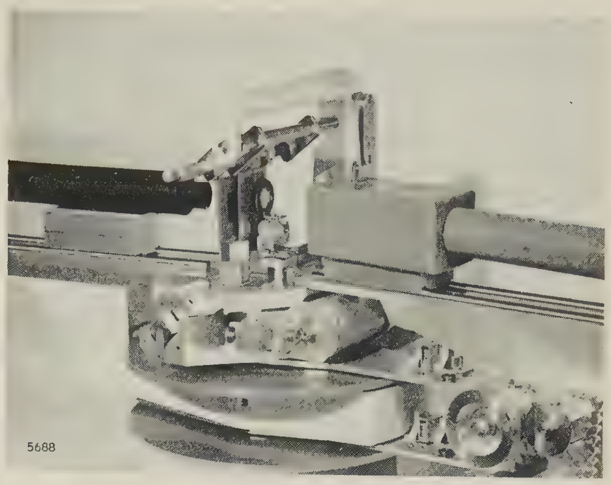

Fig. 4 *B*

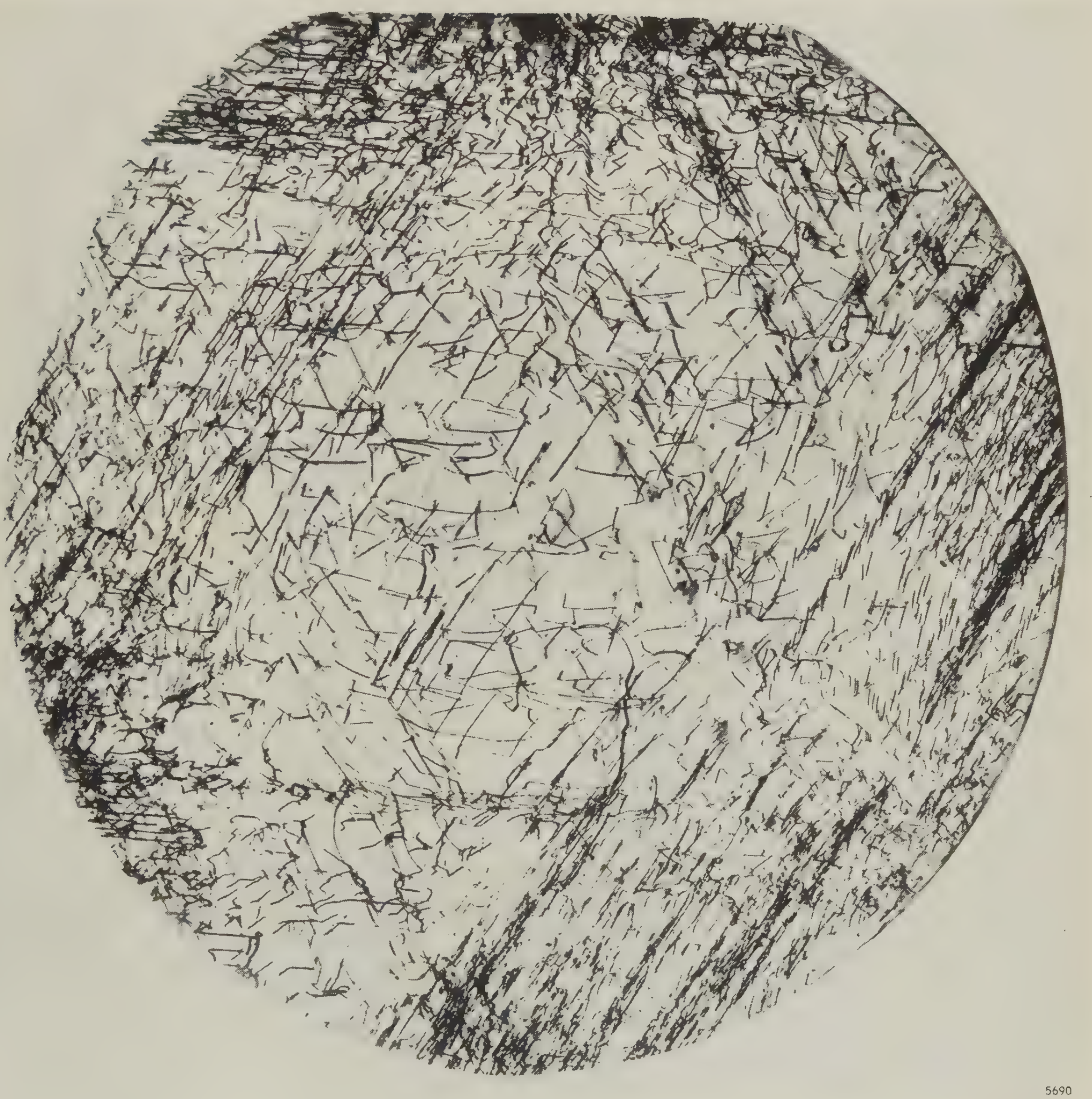

Fig. 5 *A*

to the film of the topographical details within the bulk of the crystal slice, as explained by fig. 6. The difference in projection is analogous to the difference obtained in visual observation when viewing one object from two slightly different angles. Hence, the two projection topographs form a stereo pair, which after suitable enlargement may be studied with the aid of a standard stereo viewer.

Fig. 7 shows an anaglyph of such a stereo pair, consisting of the topograph already shown in fig. 5, in which the Bragg reflection from the $(02\bar{2})$ plane was used, and the corresponding topograph with reflection from the $(0\bar{2}2)$ plane. The dislocations within the crystal stand out clearly when this figure is viewed through the red-blue spectacles supplied.

A little known but quite useful method of obtaining the stereoscopic effect without a stereo viewer or an anaglyph makes use of a simple mirror [7]), as shown in *fig. 8*. One picture of the stereo pair must be reproduced as its mirror image for this method to be applicable. The second topograph corresponding to fig. 5 is reproduced in this way on the accompanying loose leaf (fig. 5*A*). This method, like the anaglyph, has the advantage over the stereo viewer that the viewing distance need not be approximately equal to the distance between the eyes, so that relatively large pictures can also be observed bit by bit.

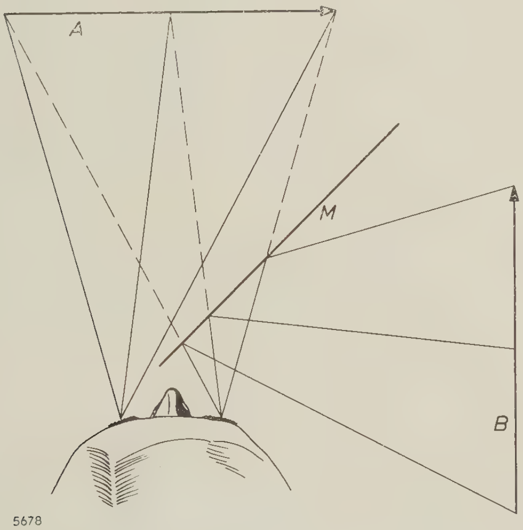

Fig. 8. Stereoscopic viewing with the aid of a simple mirror [7]). *A* and *B* are the stereo pair to be viewed; *B* must be reproduced as a mirror image. *M* is the mirror (preferably a metal one, to avoid double images). One "looks" with both eyes at one of the pictures (in this case *A*), but in fact the right eye receives the mirror image of *B*. The two images which are observed can be made to fuse into one by suitable adjustment of *B* and/or *M*.

The reader who wants to try this method of viewing will probably find it useful to practice with a photograph of a normal object first. Fig. 4 is therefore also reproduced as a stereo pair (fig. 4*A*, *B*) on the loose leaf.

Additional information on the dislocations in a crystal slice may be obtained by comparing several projection topographs of the same region, produced by reflection from *different lattice planes*. With anisotropic distortions of the lattice such as screw and edge dislocations, the mechanism giving rise to an enhanced reflection intensity and rendering the imperfection visible will not be equally effective for all directions of the primary and reflected beam.

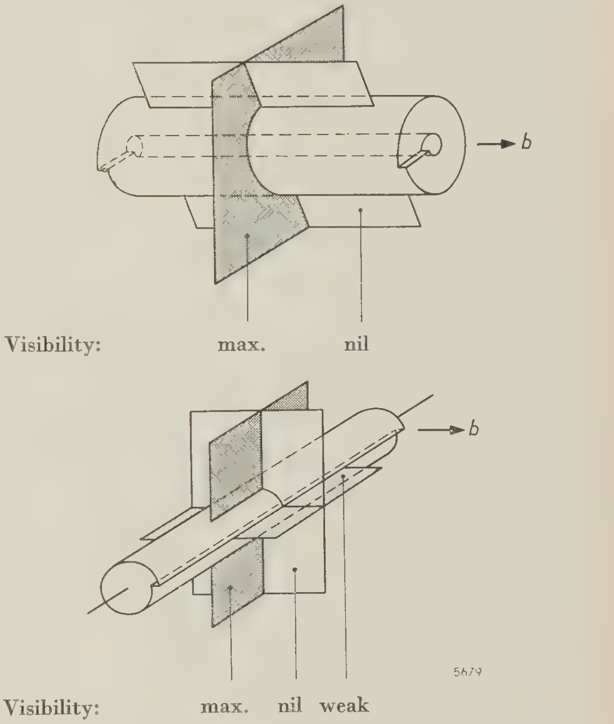

Fig. 9. Illustration of differing visibility of a dislocation in a projection topograph according to the orientation of its Burgers vector *b* with respect to the reflecting lattice plane.

Above: Screw dislocation. Reflection against the lattice plane indicated in grey will result in maximum visibility; reflection against any lattice plane oriented perpendicular to this grey plane will result in zero visibility of this dislocation.

Below: Edge dislocation. Reflection against the dark grey lattice plane yields maximum visibility; the dislocation will be weakly visible on reflection against the light grey lattice plane and it will remain invisible on reflection against the third lattice plane drawn here.

For example, the strain field around a screw dislocation is such that one would expect no X-ray image from it when its Burgers vector lies in the reflecting plane; maximum visibility would be expected when the Burgers vector is normal to the reflecting plane. Similar, although slightly more complicated, considerations apply to the edge dislocation. The result of these considerations is illustrated in *fig. 9*.

---

[7]) This method was devised by D. Brewster in 1849 (Trans. Roy. Scott. Soc. Arts **3**, 247, 1851). See also M. von Rohr, Die binokularen Instrumente, Springer, Berlin 1920, 2nd Edn., p. 62.

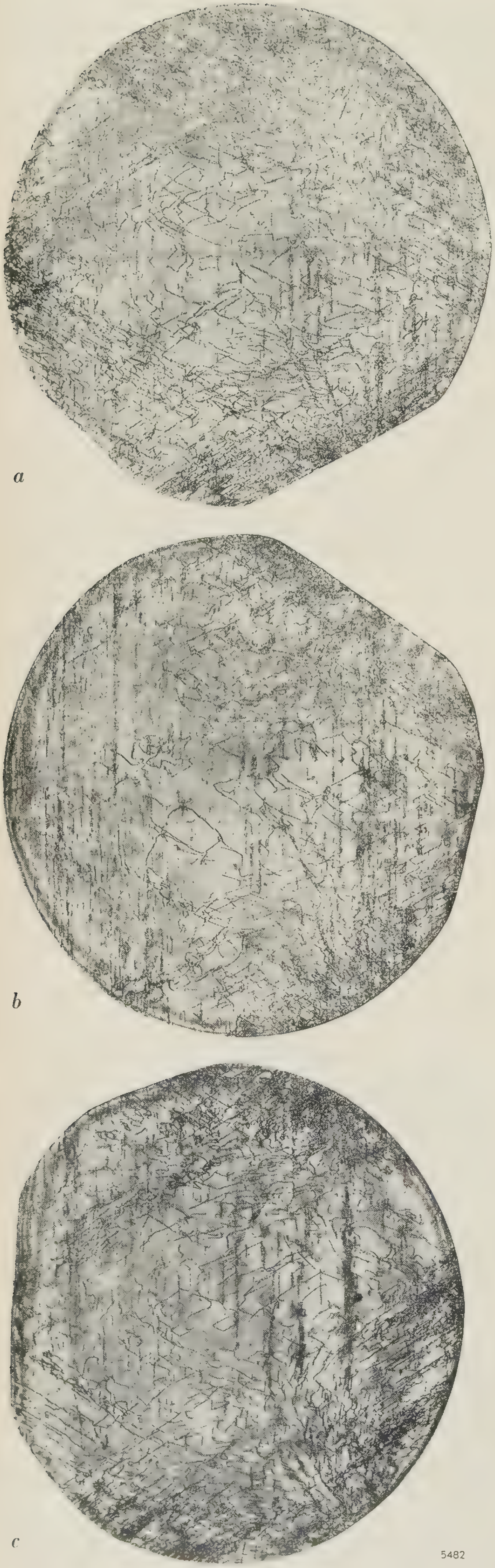

Fig. 10. Three projection topographs of the same slice as in fig. 5, made by reflection from *a*) the $(11\bar{1})$ plane, *b*) the $(1\bar{1}1)$ plane, *c*) the $(\bar{1}11)$ plane. The photographs illustrate the varying visibility of individual dislocations when different reflections are used.

The high density of dislocations at the boundary of the slice suggests the existence of dislocation sources in or near the crystal surface. Because of the relatively high density it is difficult to identify them and also to distinguish "grown-in" dislocations.

In *fig. 10* are shown three different projection topographs of the slice of silicon used for fig. 5: the lattice planes used were the $(11\bar{1})$, $(1\bar{1}1)$ and $(\bar{1}11)$ octahedral planes, the plane of the slice being (111). Now in silicon, the Burgers vectors lie in $\langle 110\rangle$ directions. Hence, in a given $\{111\}$ reflection, a dislocation with any one of the three possible $\langle 110\rangle$ Burgers vectors (either positive or negative) *not* lying in the $\{111\}$ plane is strongly visible, whereas a dislocation with any one of the three other $\langle 110\rangle$ Burgers vectors which *do* lie in the $\{111\}$ plane is invisible or almost so. It can therefore be concluded that a dislocation which is invisible in any *two* of the pictures of fig. 10 will have as its Burgers vector the direction of intersection of the two reflecting planes used. Thus, dislocations invisible in figs 10*a* and 10*b* but visible in fig. 10*c* have a Burgers vector in the direction [011]. Dislocations invisible in only *one* of the three topographs have a Burgers vector which is parallel to the direction of intersection of that particular reflecting plane and the (111) plane of the slice.

Summary. The method of projection topography of thin slices of single crystals by means of diffracted X-rays, as devised by Lang, is explained and a number of topographs are shown. The distribution of dislocations within a crystal is beautifully revealed by stereo pairs of projection topographs, and topographs of one slice made by diffraction from different lattice planes allow the identification of each dislocation according to the orientation of its Burgers vector.

OPTICAL MEASUREMENT OF RECORDED VELOCITIES ON STEREOPHONIC TEST RECORDS

by C. R. BASTIAANS *) and J. van der STEEN *).

53.082.531:681.854

Some thirty years ago it was shown that a simple relation exists between the peak lateral velocity of the cutting head in disc recording — the "peak stylus velocity" — and the width of the reflected bands of light which are observed when a beam of light is directed on to the walls of the groove in a test record. This relation offers a simple means of calibrating test records of which the peak stylus velocity must be accurately known. The results are not sufficiently reliable, however, for stereophonic disc recording. In the article below the authors derive the condition which must be fulfilled if accurate results are also to be obtained with stereodiscs, and describe an optical system of measurement incorporating the principles discussed.

In the gramophone industry, wide use is made of test records, i.e. gramophone discs on which tones of accurately known pitch have been recorded. They are also used in such electro-acoustical work as investigating the characteristics of cutting heads, pick-ups and loudspeakers.

For measurement purposes it is necessary to know precisely either the amplitude of the groove excursions on these records, or the "peak stylus velocity" (also known as the peak modulation velocity), i.e. the maximum lateral velocity of the cutter tip during the recording, which is proportional to the above-mentioned amplitude.

In 1930 Buchmann and Meyer described a simple method of measuring the stylus velocity by optical means ¹). They showed that the reflected bands of light observed when a parallel beam of light is directed on to the walls of the groove have a width b which is proportional to the peak stylus velocity $\hat{v}$, and is independent of the groove radius and the frequency of the recorded signal:

$$v = \pi n b , \qquad \qquad (1)$$

where n is the rotational speed of the record in revolutions per second during the cutting process. If $\hat{v}$ is constant, which it frequently is on test records, the reflection is observed as two diametrically opposite bands of light having a constant width b (in *fig. 1* denoted by $b_{\rm i}$ and $b_{\rm o}$). By measuring b, the value of $\hat{v}$ can be found from (1).

Using more rigorous proofs than were given by Buchmann and Meyer, we shall presently derive a more general formula, valid for both stereophonic and monophonic records ²). First of all, we shall briefly recount the various methods of modulation used for disc recording.

Methods of modulation

The essential difference between an ordinary monophonic gramophone record and a stereophonic record is that two signals are recorded on the latter — the "left-hand" and "right-hand" signals. In early experiments attempts were made to provide each signal with its own sound track, two grooves being engraved either on one side of the disc ³) or on two sides. This involved using two cutting heads and two pick-ups, and accurate synchronization proved to be an intractable problem. Moreover, it had the fundamental disadvantage of reducing the playing time of a stereodisc to half that of a monophonic disc of equal size.

In the modern stereodisc the two signals are impressed in the same groove. The cutting stylus is coupled to two driving systems, which in principle operate independently. To avoid interaction between the systems, the two directions of movement must be perpendicular to one another. The most obvious possibilities are then:

1) One signal is recorded *laterally* in the groove — as in a conventional monophonic disc — and the other *vertically*, i.e. on the "hill-and-dale" principle common half a century ago. This is known as the "0/90" method. The directions in which the wall of the groove moves in lateral and vertical modulation can be seen in *fig. 2a* and *b*.

---

*) Philips Phonographic Industries, Baarn, the Netherlands.

¹) G. Buchmann and E. Meyer, Eine neue optische Messmethode für Grammophonplatten, Elektr. Nachr.-Techn. **7**, 147-152, 1930. A shortened form of this article has appeared in English: J. Acoust. Soc. Amer. **12**, 303-306, 1940.

²) We are indebted for this derivation to H. de Lang of Philips Research Laboratories, Eindhoven.

³) K. de Boer, Experiments with stereophonic records, Philips tech. Rev. **5**, 182-186, 1940.

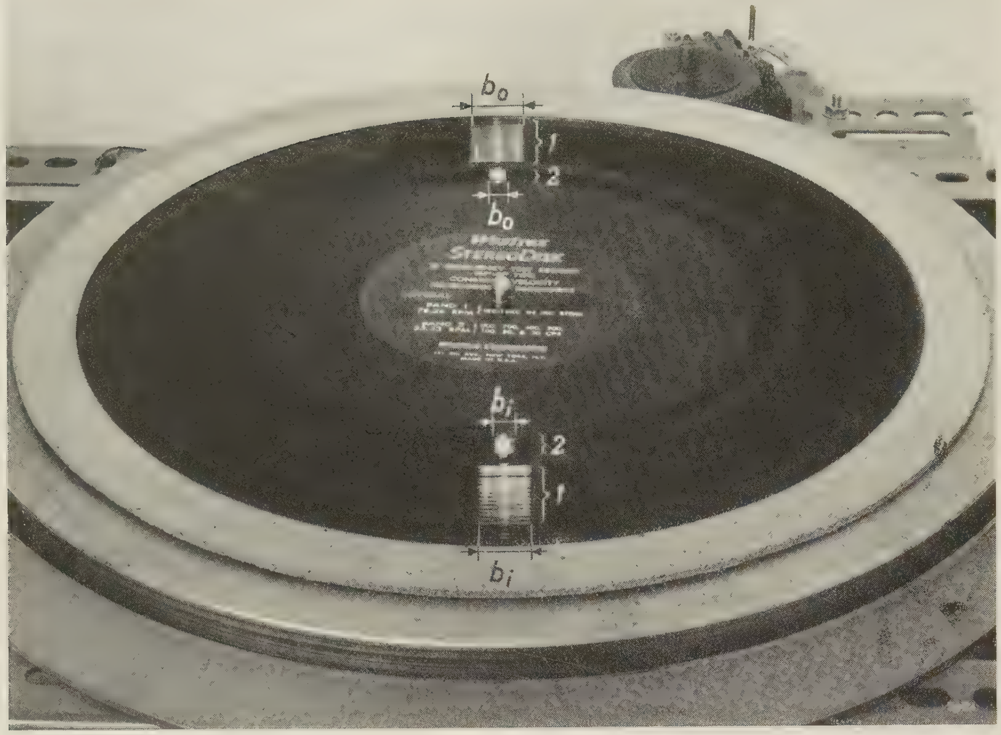

Fig. 1. On this test record a series of sine waves of different frequencies are recorded, in the turns *1* at 78.26 r.p.m. and in the turns *2* at 33.33 r.p.m. The peak stylus velocity is constant in each set of turns, but is lower in *2* than in *1*. Two diametrically opposite bands of light can be seen on each set of turns. In agreement with equation (1), the width of these bands is constant. (The difference between the width b_i on the front half and the width b_o on the rear half of the record is negligible to a first approximation.) For further particulars of this record see fig. 10.

2) Both signals are recorded symmetrically, the two cutting angles being 45° with respect to the surface of the disc. This is known as "45/45" or *45° modulation*. If only one of the two signals is present, then only one of the two groove walls is modulated (fig. 2*c*).

One advantage of the 45/45 method is that laterally it gives a summation of the two signals, so that the record can be played monophonically with a normal pick-up responsive to lateral movement only [4]). Nowadays, therefore, all stereophonic records are produced by the 45/45 method. Some test records, however, are modulated by the 0/90 system for the purpose of investigating certain characteristics of stereophonic pick-ups for 45°-modulated discs.

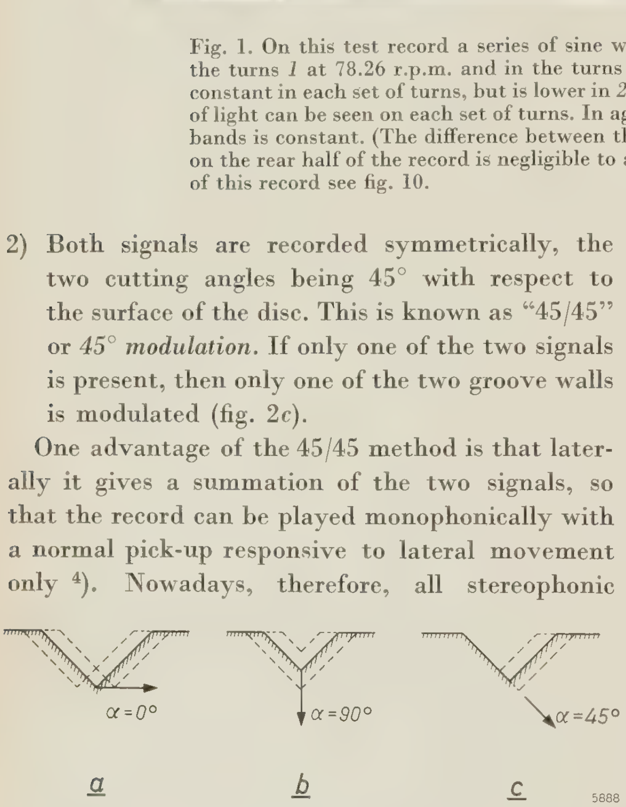

Fig. 2. Displacement of the walls of a groove (seen in axial cross-section) when *a*) laterally modulated, *b*) vertically modulated, and *c*) 45°-modulated. The arrow indicates the cutting direction of the stylus point. The angle made by the arrow with the plane of the disc is the cutting angle (0°, 90° and 45°, respectively).

In both methods it is possible in principle to keep the two signal channels entirely distinct. In practice, however, some degree of cross-talk is inevitable. Cross-talk causes distortion of the stereophonic sound picture and depends on the geometry of the cutting stylus and pick-up [5]). With the light-pattern system of measurement it is possible to determine not only the stylus velocity but also, in principle at least, the degree of cross-talk in so far as it is due to the cutting head and is thus "in the record", and not "in the pick-up".

Derivation of the relation between the light-band width, the peak stylus velocity and various other parameters

The relation between the observed width b of the band of light and the peak stylus velocity $\hat{v}$, which is the maximum value of the sinusoidally varying stylus velocity v, depends in general on two angular parameters: the cutting angle α (see fig. 2) and the angle of incidence of the light β, which is at the same time the angle of observation. Both angles are measured with respect to the plane of the disc[6].

---

[4]) The moving system of this (monophonic) pick-up must possess adequate compliance in the vertical direction to avoid damage to the vertical groove-modulation in the stereodisc.

[5]) J. L. Ooms and C. R. Bastiaans, Some thoughts on geometric conditions in the cutting and playing of stereodiscs and their influence on the final sound picture, J. Audio Engng. Soc. 7, 115-121, 1959.

For the sake of convenience we introduce a third parameter, i.e. the angle φ in *fig. 3*, which can be expressed directly in terms of b:

$$\sin\varphi = b/2R, \qquad \ldots\ldots \quad (2)$$

where R is the radius of the modulated groove (we shall for the moment consider only one turn of the groove). 2φ is the angle subtended at the centre M by the outermost reflecting points A_1 and A_2 in this turn.

For simplicity we assume that geometrical optics are applicable to this case, which enables us to disregard diffraction effects. We can further simplify the problem by imagining the groove to be cut not in a rotating disc by a stylus moving only in a lateral direction, but in a stationary disc by a stylus which not only has a lateral motion but also rotates about the centre of the disc (at a rate of n revolutions per second). In the absence of modulation the stylus then has simply a "groove velocity" V, given by

$$V = 2\pi R\,n. \qquad \ldots\ldots \quad (3)$$

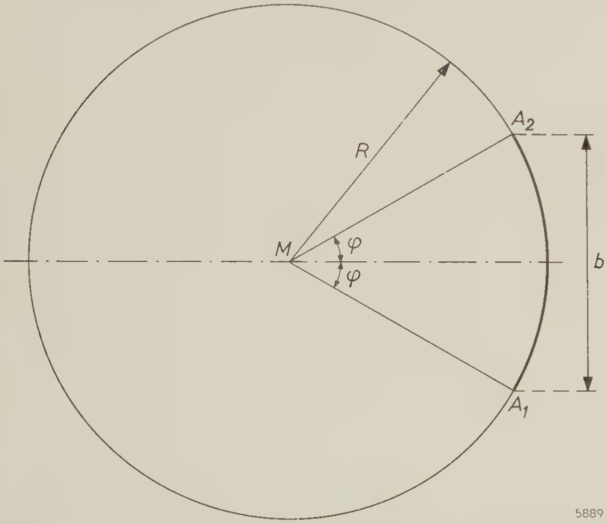

Fig. 3. In the turn of a groove of radius R only the thickly drawn portion A_1A_2 contains points that reflect light in the direction of the observer. A_1 and A_2 are the outermost points of reflection, b is the width of the band of light observed on successive turns.

The light incident at an angle β will be reflected in the same direction only by certain points in the groove, i.e. only by those points where the normal makes an angle β with the plane of the disc. *Fig. 4* shows a cross-section of the groove perpendicular to the resultant motion of the stylus point (the resultant motion being the vector sum of the velocities V and v). In this cross-section the bottom of the groove has a set of normals lying in the plane of the drawing with directions bounded by the normals n_1 and n_2. The condition for reflection in the direction β is not only that β should lie between n_1 and n_2 but also that it should be in the plane perpendicular to the direction of the resultant motion of the stylus.

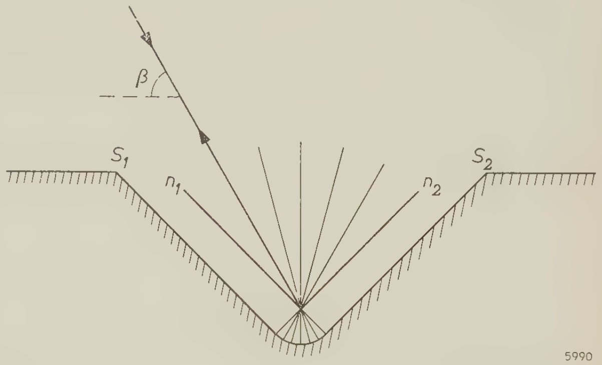

Fig. 4. Cross-section of a groove in a plane perpendicular to the resultant motion of the stylus point. The bottom of the groove has a set of normals limited by n_1 and n_2. Light will be reflected in the viewing direction β along one of these normals provided the plane of the cross-section is parallel to that direction.

The farther the points that reflect light in the required direction are removed from the vertical plane of symmetry of the observed band of light, the larger is the angle which the resultant stylus motion makes with the linear motion at the position of these points at the bottom of the groove (*fig. 5*). The outermost points that still reflect light in the direction β, A_1 and A_2, are therefore those where this angle is maximum, i.e. where the tangent of

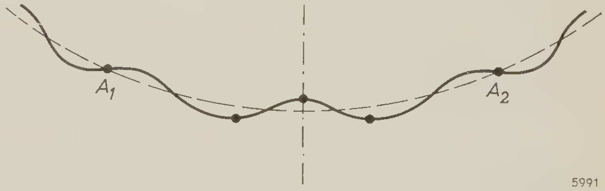

Fig. 5. The undulating line represents the bottom of the groove (seen from above), the dots are the points that reflect light in the direction of observation. The farther these points are from the plane of symmetry, the steeper is the portion of the undulating line on which they are located. At the outermost points of reflection, A_1 and A_2, the undulating line has its maximum slope in relation to the unmodulated groove. To the left of A_1 and the right of A_2 the observer sees no reflections.

---

[6] The direction of incidence need not coincide with the direction of observation. Where they are different, the theory given here still holds if β is understood to be the angle which the bisectrix of the angle between the two directions makes with the plane of the disc. We shall confine ourselves here to the case where the two directions do coincide, as they do in the measuring equipment to be described below.

the angle is equal to $\hat{v}/V$. From this we can calculate $\hat{v}$ if we know the maximum angle as a function of the parameters α and β.

If conditions are such that the bottom of the groove is not visible, a band of light is still observable, of lower intensity but of the same breadth. This reflection is attributable to the fine tracks left in the walls of the groove by unavoidable irregularities in the cutting edges of the stylus. For such very fine tracks we cannot of course apply considerations of geometrical optics as we have done for the bottom of the groove. However, further analysis, taking diffraction into account, yields exactly the same result.

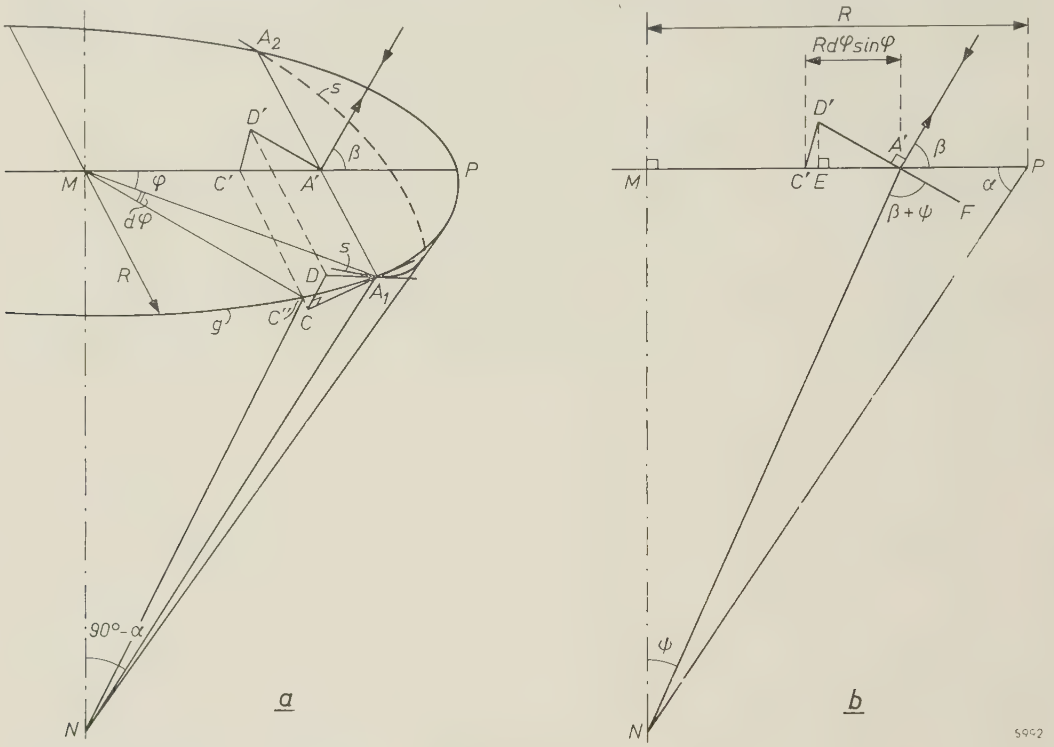

Fig. 6. *a*) The cone along which each point on the stylus cutting edges moves when cutting a groove. M centre of the disc. g turn of groove, of radius $R = MP = MA_1$. N apex of the cone (half angle 90°—α). A_1 and A_2 outermost points that reflect light in the direction of observation β. The plane through A_1A_2 perpendicular to the direction β cuts the cone in the curve s. The tangent of the maximum angle between the resultant stylus velocity $V + \hat{v}$ and the "groove velocity" V is CD/A_1C.
b) Triangle $A'C'D'$ is the projection of the triangle A_1CD in (*a*) on to the plane MNP; ψ is the projection of $\angle MNA_1$ $(= 90° - \alpha)$ on to the same plane. $\angle NA'F = \beta + \psi$.

Another limitation of the application of geometrical optics is that the "wavelength" and the amplitude of the modulation in the disc are not always sufficiently large compared with the wavelengths of the light. At a frequency of 1000 c/s, and at the usual amplitudes on test records, this gives no trouble, but at higher audio frequencies it calls for more detailed analysis [7]).

An entirely different role is played in principle by the upper edges of the groove (the lines where the groove walls intersect the plane of the disc; S_1 and S_2 in fig. 4). The upper edges do not follow the motion of the point of the stylus, but describe a curved path in the plane of the disc with an amplitude that depends on the directions of the cutting edges of the stylus as well as on the motion of its point. It is not yet known how far reflections from the upper edges are of practical significance.

We shall now calculate the tangent of the maximum angle between the resultant motion of the stylus point and the unmodulated motion (this tangent, multiplied by V, gives the peak stylus velocity $\hat{v}$).

During a recording, every point on the cutting edges of the stylus moves along the surface of a cone of half angle 90°—α (see *fig. 6a*). According to the considerations given above, at the outermost points of reflection, A_1 and A_2, the resultant motion (the vector sum of V and $\hat{v}$) is in the plane perpendicular to the direction β, and the stylus velocity $\hat{v}$ is directed along the generator of the cone. It follows that the resultant motion of the point of the stylus is tangential to the curve s in which the plane perpendicular to the direction β cuts the cone. The angle A_1MP is equal to the angle φ in fig. 3.

Our object is to find the tangent of the angle between $V + \hat{v}$ and V, i.e. the tangent of $\angle CA_1D$. This is equal to CD/A_1C, where the angle at C is a right angle. As C tends to A_1, CA_1 tends to arc $C''A_1 = R\,\mathrm{d}\varphi$, whilst simple geometrical considerations (given below in small print) show the value of CD to be:

---

[7]) B. B. Bauer, Calibration of test records by interference patterns, J. Acoust. Soc. Amer. 27, 586-594, 1955.

$$CD = R\,\mathrm{d}\varphi\,\sin\varphi\,\frac{\cos\beta\cos\psi}{\sin\alpha\sin(\beta+\psi)}, \qquad (4)$$

where the angle $\psi = \angle MNA'$ is the projection of $\angle MNA_1$ $(= 90°-\alpha)$ on the plane MNP (fig. 6*b*).

We project the triangle A_1CD on to the plane MNP. This gives the triangle $A'C'D'$ (fig. 6*b*), where $A'C' = R\,\mathrm{d}\varphi\sin\varphi$. As C and D in fig. 6*a* approach A_1, the side $A'D'$ tends to:

$$A'D' = R\,\mathrm{d}\varphi\,\sin\varphi\,\frac{\cos\psi}{\sin(\beta+\psi)}$$

and the perpendicular $D'E$ to:

$$D'E = R\,\mathrm{d}\varphi\,\sin\varphi\,\frac{\cos\psi\cos\beta}{\sin(\beta+\psi)}.$$

From this we arrive at (4), since $CD = D'E/\sin\alpha$.

The ratio CD/A_1C is thus equal to

$$\frac{\cos\beta\sin\varphi\cos\psi}{\sin\alpha(\sin\beta\cos\psi+\cos\beta\sin\psi)} = \frac{\cos\beta\sin\varphi}{\sin\alpha(\sin\beta+\cos\beta\tan\psi)}.$$

But $$\tan\psi = \frac{MA'}{MN} = \frac{\cos\varphi}{\tan\alpha},$$

so $$\frac{CD}{A_1C} = \frac{\cos\beta\sin\varphi}{\sin\alpha\sin\beta+\cos\alpha\cos\beta\cos\varphi}.$$

By equating this with $\hat{v}/V = \hat{v}/2\pi Rn$, we find:

$$\hat{v} = \pi n \times 2R\sin\varphi\,\frac{\cos\beta}{\sin\alpha\sin\beta+\cos\alpha\cos\beta\cos\varphi},$$

or, taking eq. (2) into consideration:

$$\hat{v} = \pi n b\,\frac{\cos\beta}{\sin\alpha\sin\beta+\cos\alpha\cos\beta\cos\varphi}. \qquad (5)$$

We could also eliminate the $\cos\varphi$ in the denominator by use of eq. (2), but this would lead to a complicated equation. The result is clearer if we make use of the fact that φ is always a relatively small angle, so that to the first approximation $\cos\varphi = 1$. We may therefore write:

$$\hat{v} \approx \pi n b\,\frac{\cos\beta}{\cos(\alpha-\beta)}, \quad \dots \quad (5a)$$

whilst in the general case the following series expansion applies:

$$\hat{v} = \pi n b\,\frac{\cos\beta}{\cos(\alpha-\beta)}\left[1+\frac{1}{8(1+\tan\alpha\tan\beta)}\left(\frac{b}{R}\right)^2+\dots\right], \quad \dots \quad (5b)$$

or, conversely:

$$b = B\left|\frac{\cos(\alpha-\beta)}{\cos\beta}\right|\left[1-\frac{\cos\alpha\cos(\alpha-\beta)}{8\cos\beta}\left(\frac{B}{R}\right)^2+\dots\right], \quad (6)$$

where $B = \hat{v}/\pi n$.

It is seen from (6) that b does not depend on R to a first approximation. Thus, provided the peak stylus velocity $\hat{v}$ (and hence B) is everywhere the same, successive turns of the groove each give two reflecting arcs having the same width b, and these arcs join together to form the bands of light visible in fig. 1.

Correction for the finite distance of the observer

Unless they are converged by optical means, the reflected parallel rays of light presuppose an infinitely distant observer. To an observer at a finite distance from the disc the band of light on the one half of the disc appears to be broader than on the other half. Let these breadths be b_o and b_i respectively (see fig. 1), then, as Bauer has shown [8]), b must be replaced by $2b_ob_i/(b_o+b_i)$. In the following we shall tacitly assume that this correction, where necessary, has been applied.

Special cases

It is now a simple matter to assign special values to the cutting angle α, and to investigate the manner in which the relation between b and $\hat{v}$ depends on β.

1) *Lateral modulation.* For $\alpha = 0$, equations (5b) and (6) become:

$$\hat{v} = \pi n b\left[1+\frac{1}{8}\left(\frac{b}{R}\right)^2+\dots\right]$$

and $$b = B\left[1-\frac{1}{8}\left(\frac{B}{R}\right)^2+\dots\right]. \quad \dots \quad (7)$$

In this case, then, there is no dependence on β whatsoever; where monophonic discs are concerned the angle of incidence therefore has no effect on the result. In practice the correction terms $b^2/8R^2$ and $B^2/8R^2$ are nearly always negligible compared with unity. Disregarding these terms, we arrive at the original equation (1) of Buchmann and Meyer.

2) *Vertical modulation.* For $\alpha = 90°$ it follows from (5b) and (6) that:

$$\hat{v} = \pi n b\cot\beta$$

and $$b = B|\tan\beta|. \quad \dots\dots \quad (8)$$

In this case, then, there is a marked dependence on β. The correction term is zero.

3) *45° modulation.* For $\alpha = 45°$, equations (5b) and (6) become:

$$\hat{v} = \pi n b\,\frac{\sqrt{2}}{1+\tan\beta}\left[1+\frac{1}{8(1+\tan\beta)}\left(\frac{b}{R}\right)^2+\dots\right]$$

and

$$b = B\,\frac{|1+\tan\beta|}{\sqrt{2}}\left[1-\frac{1+\tan\beta}{16}\left(\frac{B}{R}\right)^2+\dots\right]. \quad (9)$$

Here again, b and $\hat{v}$ depend on β, however for positive values of $\tan\beta$ to a lesser degree than in vertical modulation.

4) *Appropriate choice of β.* If we compare equations (7), (8) and (9), omitting the correction term, we

---

[8]) B. B. Bauer, Measurement of recording characteristics by means of light patterns, J. Acoust. Soc. Amer. **18**, 387-395, 1946.

find that for $\beta = 45°$ the same relation holds for both vertical and lateral modulation, i.e.:

$$b = \hat{v}/\pi n, \quad \ldots\ldots \quad (1)$$

and that the expression for 45° modulation differs from (1) by only a factor $\sqrt{2}$:

$$b = \hat{v}\sqrt{2}/\pi n.$$

For this reason the apparatus presently to be described has been designed for an angle of incidence and observation of 45°.

5) *Cross-talk.* Suppose that we wish to record a sinusoidal signal by 45° modulation of only one groove wall on a test record, leaving the other wall unmodulated. If the cutting angle α is exactly 45°, and assuming $\beta = 45°$, then (9) yields:

$$b_{45} = \hat{v}\sqrt{2}/\pi n$$

(disregarding the correction term). If on the other hand we make $\beta = 135°$, then with $\alpha = 45°$ we find from (9):

$$b_{135} = \text{exactly zero.}$$

However, if the cutting angle α is not exactly 45° but $45° + \varrho$, the results are:

$$b_{45} = \frac{\hat{v}}{\pi n}\sqrt{2}\cos\varrho\left[1 - \frac{1}{8}\cos\varrho(\cos\varrho - \sin\varrho)\left(\frac{\hat{v}}{\pi n R}\right)^2 + \ldots\right]$$

and

$$b_{135} = \frac{\hat{v}}{\pi n}\sqrt{2}|\sin\varrho|\left[1 + \frac{1}{8}\sin\varrho(\cos\varrho + \sin\varrho)\left(\frac{\hat{v}}{\pi n R}\right)^2 + \ldots\right].$$

A certain amount of cross-talk now exists on the second wall, the level of which is

$$10\log\left(\frac{b_{135}}{b_{45}}\right)^2 \text{dB} \quad \ldots\ldots \quad (10)$$

below that of the signal on the first wall. The amount ϱ by which the cutting angle differed from 45° is given by:

$$\tan\varrho = \frac{b_{135}}{b_{45}} \quad \ldots\ldots \quad (11)$$

(assuming that we may neglect the correction terms).

It is here in particular that interference may be expected from the reflections from the upper edges of the groove, as mentioned above. These reflections give a light-band width which does not satisfy the basic formula (6) and which is superimposed on b_{45} and b_{135}. Equations (10) and (11) must therefore be used with some caution.

Experimental verification of the theory

To verify the theory, the light-band width b was measured as a function of the angle of incidence β for a Philips test record DV 140 205. On this record the first series of turns is 45°-modulated on the inner wall ($\alpha = 45°$), the second series is 45°-modulated on the outer wall ($\alpha = 135°$), the third series is laterally modulated ($\alpha = 0°$) and the fourth series vertically modulated ($\alpha = 90°$). The stylus velocity is constant for a given series of turns, but for the third and fourth series it is greater by a factor of $\sqrt{2}$ than for the first and second series. In *fig. 7* the full lines represent the results of the measurement, and the broken lines the values calculated from equations (9), (8) and (7), neglecting correction terms. The agreement is seen to be most satisfactory.

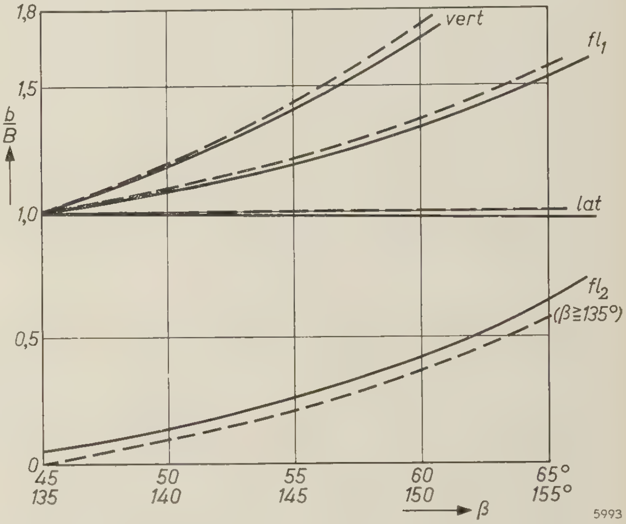

Fig. 7. Measured values (full lines) and calculated values (broken lines) of the light-band width b, divided by B, as a function of the observation angle β: *lat* for lateral modulation, *vert* for vertical modulation, fl_1 for 45° modulation (modulated groove wall), fl_2 idem (unmodulated groove wall; $\beta \geqq 135°$). The measurements were done on a Philips test record DV 140 205 ($33\frac{1}{3}$ r.p.m., recorded sinusoidal signal of frequency 1000 c/s, peak stylus velocity constant, but a factor of $\sqrt{2}$ lower for 45° modulation than for lateral and vertical modulation).

The measuring set-up

On the theoretical principles described, a measuring set-up for the calibration of test records has been constructed at Philips Phonographic Industries, Baarn. The light is incident on the record at an angle of 45°, and the reflection is observed from the same direction.

A diagram of the apparatus is shown in *fig. 8*, and a photograph in *fig. 9*. A collimator C delivers a parallel beam of light having a cross-section of 10 by 10 cm. The beam falls on the semi-reflective mirror M_1. The transmitted beam is incident on the left half of the test record G at an angle of 45° and there illuminates a rectangle measuring 10 by 14 cm which includes all the turns of the groove. The light is reflected back to the mirror M_1, which

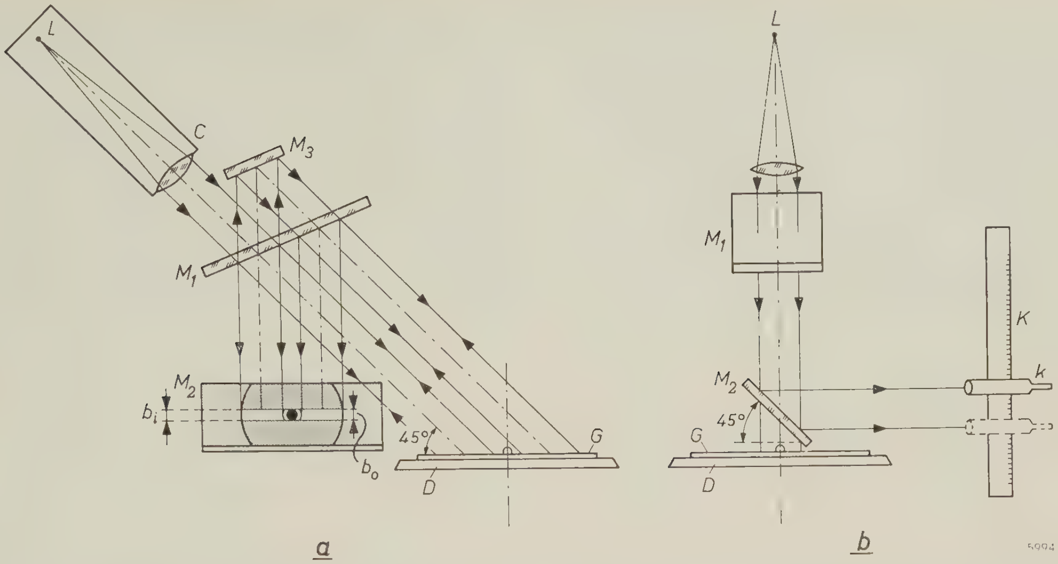

Fig. 8. Measuring set-up seen *a*) from the front, *b*) from the side. *G* record under investigation. *D* turntable. *C* collimator. M_1 semi-reflective mirror. M_2 and M_3 fully reflective mirrors. *K* cathetometer, with viewer *k*.

In the mirror M_2 two images appear side by side. The left image is from the left half of the record, the right from the right half (corresponding with the front and rear halves respectively in fig. 1). Their widths (in this arrangement their heights), b_i and b_o respectively, are measured with the cathetometer.

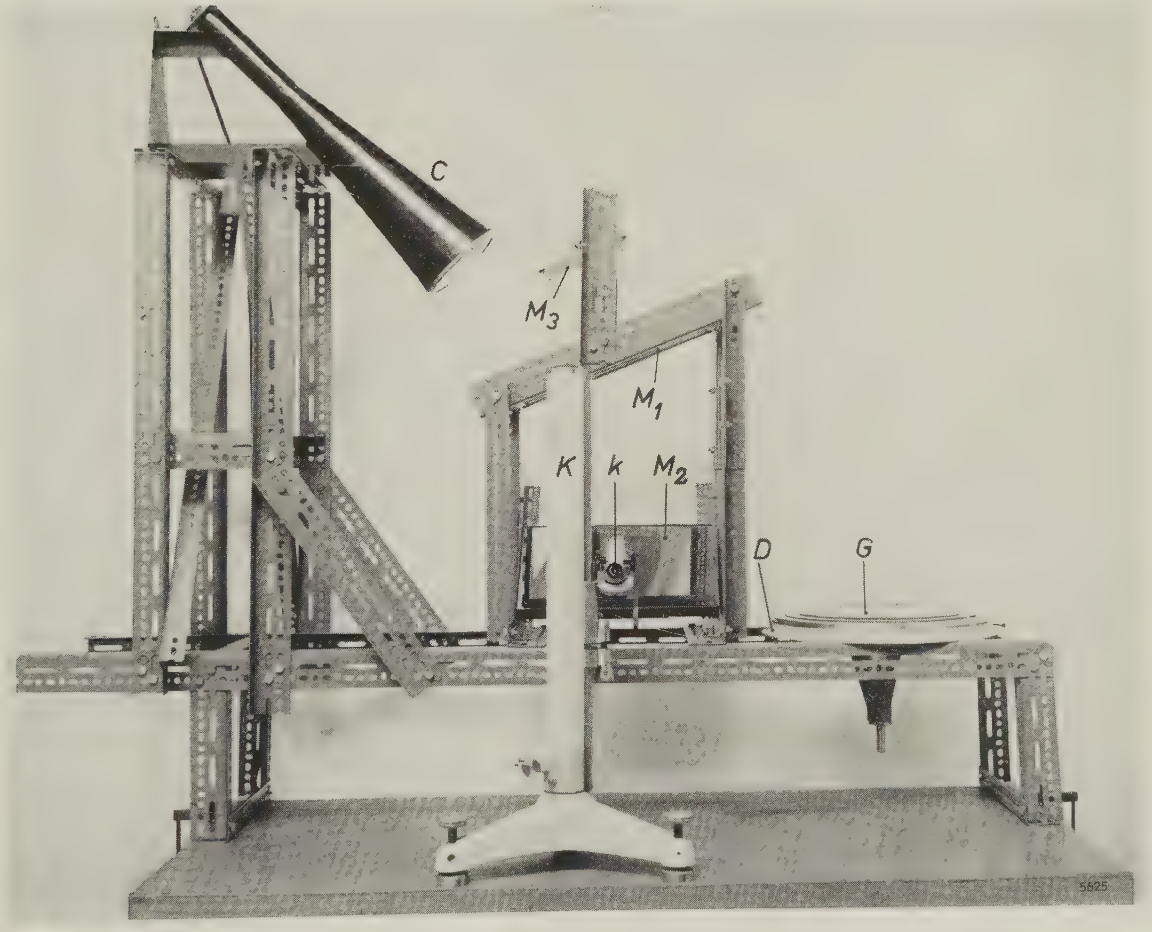

Fig. 9. Measuring set-up as in fig. 8, the letters having the same meaning. The cathetometer is 1.85 metres in front of the mirror M_2. The optical distance from the viewer to the left and right halves of the record is 2.77 and 2.85 metres respectively.

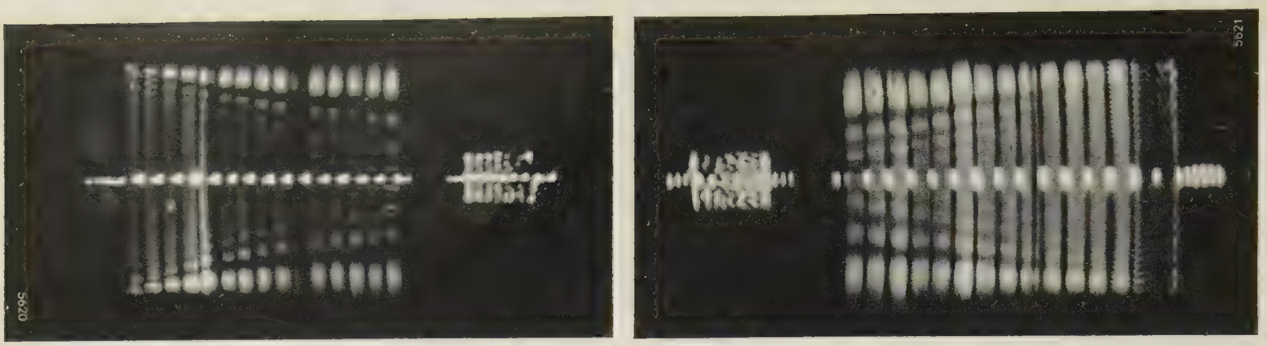

a *b*

Fig. 10. Photographs of the light patterns on the laterally modulated side of a "Westrex" test record observed in the apparatus described (the same side of this record is also to be seen in fig. 1); *a*) front (left) half, *b*) rear (right) half of record. A series of sinusoidal signals was recorded, first at 78.26 r.p.m., the pitch rising in steps of 1 kc/s from 1 to 15 kc/s, and then at 33.33 r.p.m., the pitch decreasing in steps from 1000 to 30 c/s. In both series the peak stylus velocity is seen to be reasonably constant.

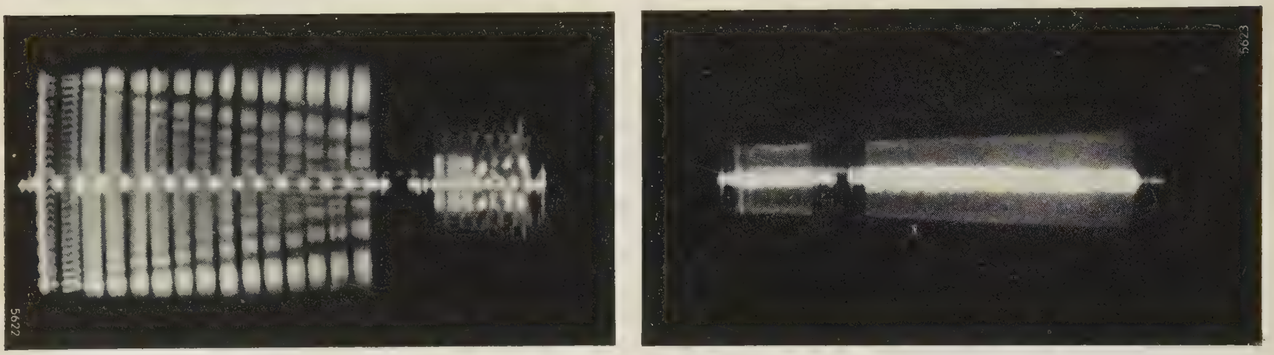

a *b*

Fig. 11. As fig. 10, now with another "Westrex" test record on which the same programme is recorded, but only on the inner wall of the groove (45° modulation). Here too the peak stylus velocity is practically constant for both series of frequencies, see (*a*). It may be seen from (*b*) that there is some cross-talk on the outer wall of the groove.

reflects part of it downwards to the ordinary (fully reflective) mirror M_2 which makes an angle of 45° with the vertical. The emergent rays are thus horizontal.

The mirror M_1 directs roughly half the light from the collimator vertically upwards. This light is reflected by the ordinary mirror M_3 at an angle of 45° on to the right half of the record, where it again illuminates a rectangle of 10 by 14 cm; β must be considered here to be 135°. The light reflected within this rectangle passes out horizontally via M_1 and M_2.

Two images are thus seen side by side in the mirror M_2: on the left the image from the left half of the record, and on the right that from the right half of the record, with $\beta = 45^\circ$ and 135° respectively. The heights of these images are the widths to be measured, b_i and b_o respectively, and they are determined (with an accuracy of up to 0.1 mm) by means of the cathetometer K, without it being necessary to shift the beam of light or the record. The cathetometer can also remain in position if a maximum error in the observation angle of $\pm 2^\circ$ is acceptable (i.e. a maximum error in $\hat{v}$ of 0.16 dB at $\alpha = 45^\circ$ or of 0.3 dB at $\alpha = 90^\circ$).

Since the mirror M_1 loses roughly half its incident light upon every reflection or transmission, a fairly high luminous flux is required from the collimator and the measurement is done in a darkened room.

If the recorded tone is fairly low, the reflecting points are seen separately. It is then desirable to let the disc rotate at about 20 revolutions per minute during the measurement. For this purpose the disc lies on a turntable.

The maximum width that can be measured in this way is 10 cm. On a 78-r.p.m. record this corresponds to a peak stylus velocity of 40.8 cm/sec, and on a $16\frac{2}{3}$-r.p.m. record to 8.7 cm/sec.

Finally some photographs are shown of the patterns produced with this set-up on two "Westrex" test records. On each side of these records a series of sinusoidal signals rising in steps of 1 kc/s from 1 to 15 kc/s is recorded at 78.26 r.p.m., followed by a series of sinusoidal signals decreasing in steps from 1000 to 30 c/s, recorded at 33.33 r.p.m. On one record this programme was recorded by lateral cut on one side and by vertical cut on the other; on the second record 45° modulation was used, on one side on the inner wall of the groove and on the other on the outer wall.

Fig. 10 relates to the laterally modulated side of the first record, *fig. 11* to the side of the second record with the signal engraved on the inner wall of the groove. Figs 10*a* and 11*a* show the pattern on the left half of the record, figs 10*b* and 11*b* the pattern on the right half. It can be seen from figs 10a, 10b and 11a that the stylus velocity was reasonably constant. Fig. 11b shows a narrow band of light, indicating the presence of some cross-talk.

Summary. In 1930 Buchmann and Meyer published an optical method of measuring the peak stylus velocity with which a sinusoidal signal is recorded on a test record. They showed that this velocity is proportional to the width of the band of light observed on the record under specific conditions. This method was adequate for laterally modulated monophonic discs (cutting angle $\alpha = 0°$), but often unsatisfactory for stereodiscs ($\alpha = 45°$). The reason was found to be that the relationship between the stylus velocity $\hat{v}$ and the light-band width b is only independent of the angle β at which the record is observed (which is at the same time the angle of incidence of the light) in the case of lateral modulation. On stereodiscs and also on vertically modulated monophonic test records ($\alpha = 90°$) the relation between $\hat{v}$ and b depends on β. A general formula is derived giving $\hat{v}$ as a function of b, α and β. If β is made 45°, Buchmann and Meyer's simple relation also holds for stereodiscs (except for a factor $\sqrt{2}$) and for vertically modulated discs. The theory has been verified experimentally.

Finally a measuring set-up is described — made and used by Philips Phonographic Industries at Baarn — in which mirrors are employed to satisfy the condition $\beta = 45°$. Some photographs are shown of the patterns observed with this apparatus.

ABSTRACTS OF RECENT SCIENTIFIC PUBLICATIONS BY THE STAFF OF N.V. PHILIPS' GLOEILAMPENFABRIEKEN

Reprints of these papers not marked with an asterisk * can be obtained free of charge upon application to Philips' Electrical Ltd., Century House, Shaftesbury Avenue, London W.C. 2, where a limited number of reprints are available for distribution.

2847: R. van Strik: Uitschieters (Sigma **6**, 10-17, 1960, No. 1). (Outliers; in Dutch.)

Using the reasoning of mathematical statistics, the author deals with the problem of "outliers". The question is examined in how far it is permissible to omit from a sample of observations those values that are widely separated from the others. The conclusion is that it is permissible only when an irregularity in the method of observation can be demonstrated, or when sufficient information is available on the form of the frequency distribution and the spread of the variable. Special attention is paid to the possibility of non-normal, i.e. skew, distributions. Instead of rejecting an extreme value a transformation of the results is more appropriate in such cases, i.e. an examination of the values of e.g. $\log x$ or x^n instead of the measured values x. The argument is illustrated by examples.

2848: H. Koopman and J. Daams: 2,6-dichlorobenzonitrile: a new herbicide (Nature **186**, 89-90, 1960, No. 4718).

In the course of a screening programme, the herbicidal activity of 2,6-dichlorobenzonitrile has been investigated. This compound inhibits the germination of certain types of seeds in an agar solution in concentrations of 5×10^{-5} mg/ml, and also stunts the growth of young plants. The germination of wild oats was completely inhibited by spraying with amounts of 0.5-4 kg per hectare. Seeds of rice, ground nuts, maize and sunflower showed a distinct resistance. The substance is also active in vapour form. Its toxic effect on warm-blooded animals is low. The acute oral 50% lethal dose (LD50) for mice is greater than 6 g per kg body-weight, and the acute intraperitoneal LD50 is >3 g/kg. A full account of these investigations will be published elsewhere.

2849: N. W. H. Addink: Subnormal level of carbonic anhydrase in blood of carcinoma patients? (Nature **186**, 253, 1960, No. 4720).

In a recent paper (No. **2726**, these abstracts) the author showed that the zinc content of the blood of carcinoma patients was subnormal (a mean decrease of about 20 per cent being found). Since Zn atoms are a constituent of various metalloproteins, an investigation was made into the presence of Zn in the blood in the form of carbonic anhydrase. Analysis of blood fractions showed this to be probable. The possible effect of a subnormal level of carbonic anhydrase on the metabolism is mentioned, and the author urges an intensive study of the anti-carcinogenic activity of this substance.

2850: L. F. Defize and P. C. van der Willigen: Droplet transfer during arc welding in various shielding gases (Brit. Welding J. 7, 297-305, 1960, No. 5).

The paper reviews investigations on droplet transfer in the arc welding of steel with a consumable bare wire in a shielding gas atmosphere (CO_2 or argon). Droplet formation is studied with the aid of high-speed cinematography (3000 frames per second). In CO_2, with the wire connected to the positive pole, the wire melts obliquely and the droplets are transferred towards the side of the weld bead. This is attributed to asymmetric heating of the wire due to radiation from the pool of molten metal. The marked contraction of the plasma gives rise to noticeably coarse droplets unwanted in welding practice. This contraction is thought to be connected with the high thermal conductivity of CO_2 at arc temperature. In argon the plasma shows less contraction and no one-sided droplet transfer occurs at high currents. The fairly large anodic contact surface with argon produces finer droplets, which move axially through the arc. When the wire is connected to the negative pole, the droplets are coarse, which is attributed to the small diameter of the cathode spot. The addition of substances giving strong thermal electron emission to the surface of the wire can greatly increase the size of the cathode spot, and with argon a droplet transfer is obtained which is similar to that at the positive pole. With CO_2 it is not possible in this way to reduce the coarseness of the droplets.

2851: M. Avinor and G. Meijer: Vanadium-activated zinc and cadmium sulphide and selenide phosphors (Phys. Chem. Solids **12**, 211-215, 1960, No. 3/4).

It was known that addition of vanadium (V) kills the visible fluorescence of ZnS phosphors activated by Cu or Ag. This killing effect of V is now seen to consist of translating the emission into the infra-red, in the region of 2.0 μ, and not of dissipating the excitation energy completely into heat. The emission is also caused by V alone, but in most cases it is enhanced by Cu and Ag. It may be said that monovalent Cu and Ag behave here as co-activators of the trivalent V. The phosphors investigated were CdS, ZnS, CdSe and ZnSe, activated by V, V + Ag, V + Cu and V + Au. The spectral distributions of the emission bands were measured at 300 °K and 80 °K, a high-pressure mercury lamp with a water filter being used for excitation.

2852: G. Diemer: Power amplifiers using electro-optical effects (Electronics **33**, No. 9, 71-73, 1960).

Short review of 27 power amplifiers that can be designed to use various combinations of electric, radiative and thermal power (see also Nos. **2784** and **R 401**, these abstracts).

2853: H. Zijlstra: On magnetic annealing of a permanent magnet alloy (thesis Amsterdam, June 1, 1960).

"Ticonal" G is a magnet steel that derives its hard-magnetic properties from the presence of two finely dispersed phases. It is known that these phases occur in the form of elongated particles whose direction can be affected by a magnetic field during the heat treatment required for bringing the material into a double-phase condition.

The behaviour of this material during isothermal heat treatment in a magnetic field in the temperature range between 700 °C and 800 °C is described in this thesis.

From measurements of saturation magnetization after isothermal heat treatments it appears that the decomposition into two phases of the originally homogeneous alloy takes place very quickly and may be considered to be complete after the first few minutes.

From measurements of the magnetic anisotropy and of the mean distance between the precipitated particles while the heat treatment is going on, it appears that these quantities change their magnitude during a much longer period of time, so that they must be ascribed to changes of the shape and volume of the precipitated particles, the total quantity of each phase and its chemical composition remaining constant. The volume-diffusion process on which these changes are supposed to be based is analysed thermodynamically and related with the variations in the free energy of the fields of the magnetic dipoles about the particles and those in the free energy in the boundary plane between the phases. The diffusion equation thus obtained is applied to a model of prolate spheroids. From this, relationships are derived between the time of heat treatment and both the anisotropy and the distance between the particles, which appear to be in good agreement with the experimental results. In order to investigate the significance of this model, it is compared with a model of oblate spheroids. The behaviour of the model is found to have little sensitivity towards the type of the particles.

For comparison, surface diffusion along the boundary planes is investigated theoretically. The diffusion equations thus obtained are found not to correspond to the experimental data, so that it may be concluded that the latter process has little or no importance.

The good agreement between theory and experiments makes it possible to calculate the interfacial tension of the boundary between the phases; it appears to be very small (of the order of 1 erg cm^{-2}). The small interfacial tension is found to be of great importance for the response of a dispersion-hardening magnet steel to heat treatment in a magnetic field. It follows from the theory that the Mishima alloy, one of this group of magnet steels, which is generally believed not to become anisotropic during annealing in a magnetic field, ought certainly to exhibit this effect during heat treatment extending over a long period. This is proved by experiment.

A description of the measuring methods and arrangements is given.

2854: J. van der Ster: The production of liquid nitrogen from atmospheric air using a gas refrigerating machine (thesis Delft, June 22, 1960).

The advent of the gas-refrigerating machine has made it possible to produce small amounts of liquid air in an economical way. The present thesis describes how liquid nitrogen can be produced from atmospheric air by combining the refrigerating machine with an air-rectifying column. The author discusses in particular the design and construction of an installation capable of producing more than 4 litres of liquid nitrogen an hour. The purity of the product is 99.8-99.9%; the power consumption is 1.36 kWh/l.

The most conspicuous feature compared with other air-fractionating systems is that the air is not compressed. In consequence of this, the installation and its operation are extremely simple. Water vapour and carbon dioxide are removed from the feed by cooling the air in such a way that, in spite of the compact design, the installation can operate continuously for a week.

A detailed account is given of the automatic control of the installation, special attention being paid to the stability of the reflux. In the reflux-controlling system a vapour-bubble pump is used for returning the liquid nitrogen to the top of the column. An investigation of vapour-bubble pumps for liquid nitrogen and liquid oxygen is described in an appendix. Also included in an appendix are calculations and experiments on a hydrometer specially developed for simply and accurately measuring the purity of the nitrogen product.

The installation is safeguarded against explosion risks due to accumulations of hydrocarbons; the measures adopted to this end are discussed and various measurements are described.

2855: G. Meijer and R. van der Veen: Dual effect of nightbreak light (Acta bot. neerl. **9**, 220-223, 1960, No. 2).

Experiments with Salvia occidentalis, a short-day plant, showed that red nightbreak light which normally is effective in causing a long-day effect, can under certain conditions antagonize the long-day effect of a supplemental light period, thus causing a short-day effect. This short-day effect of nightbreak light disappears when the length of the nightbreak period is increased or when it is followed by an irradiation with far red (= near infra-red).

2856: E. H. Reerink, H. F. L. Schöler, P. Westerhof, A. Querido, A. A. H. Kassenaar, E. Diczfalusy and K. C. Tillinger: A new class of hormonally active steroids (Nature **186**, 168-169, 1960, No. 4719).

Preliminary communication concerning anima and clinical experiments with new synthetic compounds. Of these compounds the C-9 hydrogen atom occupies the β configuration and the methyl group at C-10 the α configuration. Therefore the compounds prepared represent the 9β, 10α analogues of the steroids of the natural series. Some of the compounds investigated showed marked progestational activity after parenteral and oral administration. No side-effects were observed. A full report will be published elsewhere.

2857: J. Verweel and B. J. M. Roovers: Magnetic properties and conduction phenomena in pure and substituted yttrium iron garnets (Solid state physics in electronics and telecommunications, Proc. int. Conf., Brussels, June 1958, edited by M. Désirant and J. L. Michiels, Vol. 3, pp. 475-487, Academic Press, London 1960).

In the substance $Y_3Fe_5O_{12}$, which has a garnet structure, ionic substitutions of divalent or tetravalent cations can be carried out which affect the resistivity. Replacement of a small amount δ of Y^{3+} by Ca^{2+} can cause some of the iron ions to become tetravalent. In the same way replacement of δFe^{3+} by δTi^{4+} or δSi^{4+} can cause δFe^{3+} to be reduced to δFe^{2+}. Samples were prepared and some physical properties, such as the resistivity as a function of temperature and the thermoelectric power, were investigated for different values of δ. The initial (complex) permeability was measured as a function of frequency and temperature, and the dispersion mechanisms are discussed.

2858: J. Smit, F. K. Lotgering and U. Enz: Anisotropy properties of hexagonal ferrimagnetic oxides (J. appl. Phys. **31**, suppl. to No. 5, 137 S-141 S, 1960).

In hexagonal crystals of the ferroxdure type the *c* axis is the preferred direction of magnetization. A magnetic field is needed to change the alignment of the magnetization, and in that case the crystal is subjected to a torque. The torque was measured as a function of the orientation of the crystal in relation to the field applied to polycrystalline material of composition $BaCo_xTi_xFe_{12-2x}O_{19}$, with aligned crystallites. It is shown that the anomalies found in the torque curves can be explained by the marked anisotropy of the cobalt ions.

2859: M. Koedam and A. Hoogendoorn: Sputtering of copper single crystals bombarded with A^+, Kr^+ and Ne^+ ions with energies ranging from 300-2000 eV (Physica **26**, 351-352, 1960, No. 5).

Earlier reported investigations into the sputtering of monocrystalline metal surfaces by ionic bombardment are being extended to higher ion energies (see also Nos. **2767** and **2840** of these abstracts).

2860: M. P. Rappoldt: Investigations on sterols, XIV. Studies on vitamin D and related compounds, XII. The photo-isomerization of lumisterol$_2$ (Rec. Trav. chim. Pays-Bas **79**, 392-400, 1960, No. 5).

Kinetic experiments on the isomerization of lumisterol$_2$ under the influence of ultraviolet light of various wavelengths are reported. The experiments indicate that neither tachysterol$_2$ nor ergosterol are primary reaction products of lumisterol$_2$. Lumisterol$_2$ is exclusively converted into pre-ergocalciferol. The quantum yield of this reaction is 0.41 at 2537 Å.

2861: M. P. Rappoldt and E. Havinga: Studies on vitamin D and related compounds, XI. Investigations on sterols, XIII. The photoisomerization of ergosterol (Rec. Trav. chim. Pays-Bas **79**, 369-381, 1960, No. 5).

Kinetic experiments on the photoisomerization of ergosterol were carried out using different sources of light. New methods of analysis for pre-ergocalciferol and tachysterol$_2$ had to be developed. The quantum yield of the photoisomerization of ergosterol with UV light of 2537 Å was found to be 0.31 at 20 °C. This value was obtained when ether, ethanol and petroleum ether were used as solvents. Tachysterol$_2$ is not formed from ergosterol during irradiation, but originates exclusively from pre-ergocalciferol. Excited ergosterol falls back to its ground state (69%) or transforms to pre-ergocalciferol (26%) and to unidentified products (5%).

2862: M. Avinor and G. Meijer: Emission of activated cadmium selenide phosphors (J. chem. Phys. **32**, 1456-1458, 1960, No. 5).

The fluorescence spectra at 80 °K and 300 °K of CdSe activated by Cu, Au and Ag, and co-activated by trivalent metals, were investigated. The phosphors were excited by radiation from a high-pressure mercury lamp passing through a $CuSO_4$ filter. For comparison, the emission spectra of CdS with the same activators and coactivators were also investigated. The emission bands of CdSe are shifted towards the infra-red in relation to those of CdS. The silver band of CdSe turned out to be completely quenched at room temperature. Besides the activator bands (Ag 0.92 μ, Cu 1.20 μ, Au 1.45 μ, at 80 °K) a near-edge emission of CdSe was found at 0.72 μ.

2863: A. A. Aldenkamp, C. P. Marks and H. Zijlstra: Frictionless recording torque magnetometer (Rev. sci. Instr. **31**, 544-546, 1960, No. 5).

An instrument for measuring magnetic anisotropy by recording magnetic torque curves is described. The special construction of the transducer which converts the torque exerted on the sample into an electrical signal makes it possible to avoid bearings, so that the instrument is essentially free of friction. The instrument is operated with commercially available electronic apparatus and is suitable for routine measurements on large numbers of samples. The maximum sensitivity is 1.5×10^{-5} Nm ($= 150$ dyne cm) per centimetre deflection of the recorder stylus.

2864: F. J. Schijff: Safety and reliability in the instrumentation of nuclear reactors (Revue HF Tijdschrift **4**, 223-229, 1960, No. 10).

The instrumentation of a nuclear reactor involves the use of instruments which are relatively unsafe and unreliable. Nevertheless, a reactor is required to possess a high degree of safety and great reliability, the first principally to protect life and property, the second mainly for reasons of economy. Both safety and reliability can be improved by means of coincidence circuits. Other measures of particular importance to safety are regular testing of the safety channels and constant comparison of the signals from identical channels.